B3.2
Quantum structural methods for the solid state and surfaces

Frank Starrost and Emily A Carter

B3.2.1 Introduction

We are entering an era when condensed matter chemistry and physics can be predicted from theory with increasing realism and accuracy. This is particularly important in cases where experiments lead to ambiguous conclusions, for regimes in which there still exists no experimental probe and for predictions of the properties of modern materials in order to select the most promising ones for synthesis and experimental testing. For example, continuing miniaturization in microelectronics heightens the importance of understanding of quantum effects, which computational materials theory is poised to provide, based to some degree on the methods presented here.

Our intention is to give a brief survey of advanced theoretical methods used to determine the electronic and geometric structure of solids and surfaces. The electronic structure encompasses the energies and wavefunctions (and other properties derived from them) of the electronic states in solids, while the geometric structure refers to the equilibrium atomic positions. Quantities that can be derived from the electronic structure calculations include the electronic (electron energies, charge densities), vibrational (phonon spectra), structural (lattice constants, equilibrium structures), mechanical (bulk moduli, elastic constants) and optical (absorption, transmission) properties of crystals. We will also report on techniques used to study solid surfaces, with particular examples drawn from chemisorption on transition metal surfaces.

In his chapter on the fundamentals of quantum mechanics of condensed phases (A1.3), James R Chelikowsky introduces the plane wave pseudopotential method. Here, we will complement his chapter by introducing in some detail tight-binding methods as the simplest pedagogical illustration of how one can construct crystal wavefunctions from atomic-like orbitals. These techniques are very fast but generally not very accurate. After reviewing some of the efforts made to improve upon the local density approximation (LDA, explained in A1.3), we will discuss general features of the technically more complex all-electron band structure methods, focusing on the highly accurate but not very fast linear augmented plane wave (LAPW) technique as an example. We will introduce the idea of orbital-free electronic structure methods based directly on density functional theory (DFT), the computational effort of which scales linearly with size, allowing very large systems to be studied. The periodic Hartree–Fock (HF) method and the promising quantum Monte Carlo (QMC) techniques will be briefly sketched, representing many-particle approaches to the condensed phase electronic structure problem.

In the final section, we will survey the different theoretical approaches for the treatment of adsorbed molecules on surfaces, taking the chemisorption on transition metal surfaces, a particularly difficult to treat yet extremely relevant surface problem [1], as an example. While solid state approaches such as DFT are often used, hybrid methods are also advantageous. Of particular importance in this area is the idea of embedding,

For an overview of Professor Carter's group's work using pseudospectral methods, see:
Martinez T J and Carter E A 1995 Pseudospectral methods applied to the electron correlation problem *Modern Electronic Structure Theory* vol 2, ed D R Yarkony (Singapore: World Scientific) pp 1132–65

[75] Hylleraas E A and Undheim B 1930 *Z. Phys.* **65** 759
MacDonald J K L 1933 Successive approximations by the Rayleigh–Ritz variation method *Phys. Rev.* **43** 830–3

[76] Pople J A 1973 Theoretical models for chemistry *Energy, Structure, and Reactivity* ed D W Smith and W B McRae (New York: Wiley) p 51–67

[77] Roos B O, Taylor P R and Siegbahn P E M 1980 A complete active space SCF method (CASSCF) using a density matrix formulated super-CI approach *Chem. Phys.* **48** 157–73
Roos B O 1987 The complete active space self-consistent field method and its applications in electronic structure calculations *Adv. Chem. Phys.* **69** 399–445

[78] Kelly H P 1963 Correlation effects in atoms *Phys. Rev.* **131** 684–99

[79] Good early overviews of the electron propagator (that is used to obtain IP and EA data) and of the polarization propagator are given in:
Jørgensen P and Simons J 1981 *Second Quantization Based Methods in Quantum Chemistry* (New York: Academic)
The very early efforts on these methods are introduced in:
Linderberg J and Öhrn Y 1973 *Propagator Methods in Quantum Chemistry* (New York: Academic)
More recent summaries include:
Cederbaum L S and Domcke W 1977 Theoretical aspects of ionization potentials and photoelectron spectroscopy a Green's function approach *Adv. Chem. Phys.* **36** 205–344
Oddershede J 1987 Propagator methods *Adv. Chem. Phys.* **69** 201–39
Ortiz J V 1997 The electron propagator picture of molecular electronic structure *Computational Chemistry: Reviews of Current Trends* vol 2, ed J Leszczynski (Singapore: World Scientific) pp 1–61

[80] The introduction of EOMs for energy differences and for operators that connect two states appears first in the nuclear physics literature; see for example:
Rowe D J 1968 Equation-of-motion method and the extended shell model *Rev. Mod. Phys.* **40** 153–66
I applied these ideas to excitation energies in atoms and molecules in 1971; see equation (2.1)–(2.6) in:
Simons J 1971 Direct calculation of first- and second-order density matrices. The higher RPA method *J. Chem. Phys.* **55** 1218–30
In 1973, the EOM method was then extended to treat IP and EA cases:
Simons J 1973 Theory of electron affinities of small molecules *J. Chem. Phys.* **58** 4899–907
In a subsequent treatment from the time-dependent response point of view, connection with the Greens function methods was made:
Simons J 1972 Energy-shift theory of low-lying excited electronic states of molecules *J. Chem. Phys.* **57** 3787–92
A more recent overview of much of the EOM, Greens function, and propagator field is given in:
Oddershede J 1987 Propagator methods *Adv. Chem. Phys.* **69** 201–39

[81] Olsen J and Jørgensen P 1995 Time-dependent response theory with applications to self-consistent field and multiconfigurational self-consistent field wave functions *Modern Electronic Structure Theory* vol 2, ed D R Yarkony (Singapore: World Scientific) pp 857–990

[82] A good overview of the recent status is given in:
Bartlett R J 1995 Coupled-cluster theory: an overview of recent developments *Modern Electronic Structure Theory* vol 2, ed D R Yarkony (Singapore: World Scientific) pp 1047–131

[83] Helgaker T, Gauss J, Jørgensen P and Olsen J 1997 The prediction of molecular equilibrium structures by the standard electronic wave functions *J. Chem. Phys.* **106** 6430–40
for a listing and for further details on this study

[84] Two review papers that introduce and compare the myriad of semi-empirical methods:
Stewart J J P 1991 Semiempirical molecular orbital methods *Reviews in Computational Chemistry* vol 1, ed K B Lipkowitz and D B Boyd (New York: VCH) pp 45–81
Zerner M C 1991 Semiempirical molecular orbital methods *Reviews in Computational Chemistry* vol 2, ed K B Lipkowitz and D B Boyd (New York: VCH) 313–65
A very recent overview, including efforts to interface semi-empirical electronic structure with molecular mechanics treatments of some degrees of freedom is given by:
Thiel W 1996 Perspectives on semiempirical molecular orbital theory *New Methods in Computational Quantum Mechanics (Adv. Chem. Phys. XCIII)* ed I Prigogine I and S A Rice (New York: Wiley) pp 703–57
Earlier texts dealing with semi-empirical methods include:
Pople J A and Beveridge D L 1970 *Approximate Molecular Orbital Theory* (New York: McGraw-Hill)
Murrell J N, Kettle S F A and Tedder J M 1965 *Valence Theory* 2nd edn (London: Wiley)

where a small cluster of surface atoms around the adsorbate is treated with more care than the surrounding region. The advantages and disadvantages of the approaches are discussed.

B3.2.2 Tight-binding methods

B3.2.2.1 Tight binding: from empirical to self-consistent

The wavefunction in a solid can be thought to originate from two different limiting cases. One extreme is the nearly free electron (NFE) approach. The idea here is that the valence electrons are hardly affected by the periodic potential of the atomic cores. Their wavefunctions can then be assumed to be easily described as linear combinations of the solutions for free electrons: the plane waves, $\exp(i\boldsymbol{k}\cdot\boldsymbol{r})$. The NFE approximation is particularly useful for so-called NFE metals, such as the alkali metals. At the other extreme, the solid can be viewed as constructed from individual atoms. The valence wavefunctions of the solid are then approximated as linear combinations of the wavefunctions of the valence electrons of the atoms (see also section A1.3.5.6). In this case, the electrons are considered to be 'tightly bound' to the atoms. This is a physically reasonable view of covalently bound solids and molecules, where localized chemical bonds are the norm (bulk silicon, organic or biomolecules etc). Methods which employ this view of the electrons in the solid are called tight-binding (TB) methods. The wavefunctions are generally expanded in atomic orbitals (in a linear combination of atomic orbitals (LCAO) formalism) or similarly localized functions.

An advantage of TB is that generally the number of basis functions linearly combined to give the wavefunctions is rather small. The solution of the Schrödinger equation in these bases is then fast because the matrices representing the operators are small. Also, the construction of the Hamiltonian matrix elements is fast, since generally a number of, sometimes drastic, approximations are made. At the same time, however, the small basis set generally limits the quality of the TB results, since the variational freedom for the solution of the Schrödinger equation is not as high as in other methods. The approximations of Hamiltonian matrix elements often further reduce the quality of the results.

Today, the term TB method is generally understood to refer to a technique using TB basis functions in which the Hamiltonian matrix elements are adjusted to reproduce results from experiments and/or from more sophisticated electronic structure methods [2]. Depending on the degree of dependence on external parameters, the methods are called empirical or semi-empirical TB. A number of approaches are used for the fitting of the TB parameters, generally a tough minimization task with many minima (using genetic algorithms has proved quite efficient [3, 4]). It has been noted that 'great care is needed to test the resulting model for reasonable behavior outside the range of the fit' [5, 6]. A disadvantage of the empirical methods is that it is difficult to distinguish to what extent the parametrization or the method itself is responsible for errors in the results.

Frequent approximations made in TB techniques in the name of achieving a fast method are the use of a minimal basis set, the lack of a self-consistent charge density, the fitting of matrix elements of the potential, the assumption of an orthogonal overlap matrix, a cut-off radius used in the integration to determine matrix elements, and the neglect of matrix elements that require three-centre integrals and crystal-field terms. We will now provide more details on these approximations.

Generally, the following *ansatz* for the wavefunction is made:

$$\psi_i(\boldsymbol{r}) = \sum_{\alpha l} c^i_{\alpha l}\varphi_{\alpha l}(\boldsymbol{r}),$$

where $\varphi_{\alpha l}(\boldsymbol{r}) = \langle \boldsymbol{r}|\varphi_{\alpha l}\rangle$ represents an atomic orbital of symmetry α (such as s, p_x, p_y, p_z) at atom l.

This yields the generalized eigenvalue problem

$$\underline{H}\boldsymbol{c}^i = \epsilon_i \underline{S}\boldsymbol{c}^i, \tag{B3.2.1}$$

with the elements of the Hamiltonian matrix $H_{\alpha l \beta m} \equiv \langle \varphi_{\alpha l} | H | \varphi_{\beta m} \rangle$ and the overlap matrix $S_{\alpha l \beta m} \equiv \langle \varphi_{\alpha l} | \varphi_{\beta m} \rangle$. In the TB approximation, the basis functions are thought to be sufficiently localized such that contributions to the Hamiltonian matrix usually are accounted for only up to at most the third or fourth neighbour. Frequently a minimal basis set is used, i.e. a single orbital $\varphi_{\alpha l}$ is used per atom and per orbital symmetry to expand the wavefunction.

In orthogonal TB methods, the overlap matrix is assumed to be diagonal, even though the basis functions of adjacent sites ordinarily are not orthogonal [6]. Harrison has shown that this approximation can be compensated for by adjustments to the Hamiltonian matrix elements (these adjustments are arrived at automatically in methods depending on fitting, for example, a DFT band structure) [7]. However, this approach reduces the transferability of the TB parameters to other structures [8]. Including the overlap matrix brings with it the additional cost of its calculation and solving the generalized eigenvalue problem, see equation (B3.2.1), rather than an ordinary eigenvalue problem.

One can construct an effective potential, written here in the DFT language (see, for example, equation A1.3.38 of A1.3) as

$$v_{\mathrm{eff}}(r) = v_{\mathrm{ext}}(r) + v_{\mathrm{H}}[\rho(r)] + v_{\mathrm{xc}}[\rho(r)]. \tag{B3.2.2}$$

To rationalize the 'two-centre approximation', the effective potential is written as

$$v_{\mathrm{eff}}(r) = \sum_l v_{\mathrm{eff},l}(|r - R_l|),$$

where $v_{\mathrm{eff},l}$ is centred on the atom l and vanishes away from the atom, which need not involve any approximation.

In the calculation of the elements

$$H_{\alpha l \beta m} = \left\langle \varphi_{\alpha l} \middle| T + \sum_n v_{\mathrm{eff},n} \middle| \varphi_{\beta m} \right\rangle$$

with $T = -\frac{1}{2}\nabla^2$ the kinetic energy operator, several types of potential matrix elements can be distinguished [6]:

(1) Three-centre terms, i.e. $l \neq m \neq n$. These are frequently neglected, in what is called the two-centre approximation, based on the assumed strong localization of the orbitals $\varphi_{\alpha l}(r)$.

(2) Inter-atomic two-centre matrix elements $\langle \varphi_{\alpha l} | v_{\mathrm{eff},l} + v_{\mathrm{eff},m} | \varphi_{\beta m} \rangle$. These matrix elements represent the hopping of electrons from one site to another. They can be described [7] as linear combinations of so-called Slater–Koster elements [9]. The coefficients depend only on the orientation of the atoms l and m in the crystal. For elementary metals described with s, p, and d basis functions there are ten independent Slater–Koster elements. In the traditional formulation, the orientation is neglected and the two-centre elements depend only on the distance between the atoms [6]. (In several models [6, 10], they have been made dependent on the environment of the atoms l and m.) These elements are generally fitted to reproduce DFT results such as the band structure or the values of DFT matrix elements in diatomics.

(3) Intra-atomic matrix elements, or on-site terms, with $l = m$. Traditionally, the potential contributions from other atomic sites, $v_{\mathrm{eff},n\neq l=m}$, so-called crystal-field terms, are neglected [10]. In this case, then the only non-zero on-site terms have $\alpha = \beta$, since basis functions on the same site are orthogonal atomic orbitals. There are methods which include these crystal-field terms [11, 12]. Physically, these diagonal elements represent the energy required to place an electron in a specific orbital. In some implementations, they are set to the orbital energy values of the neutral free atom [13], guaranteeing the correct limit for isolated atoms. However, this approach ignores the potential contributions to the diagonal elements due to different environments in a molecule or crystal; these are taken into account in other variants of the method [6, 10, 11].

Most TB approaches are not charge self-consistent. This means that they do not ensure that the charge derived from the wavefunctions yields the effective potential v_{eff} assumed in their calculation. Some methods have been developed which yield charge densities consistent with the electronic potential [14–16].

The localized nature of the atomic basis set makes it possible to implement a linear-scaling TB algorithm, i.e. a TB method that scales linearly with the number of electrons simulated [17]. (For more information on linear scaling methods, see section B3.2.3.3.)

The accuracy of most TB schemes is rather low, although some implementations may reach the accuracy of more advanced self-consistent LCAO methods (for examples of the latter see [18–20]). However, the advantages of TB are that it is fast, provides at least approximate electronic properties and can be used for quite large systems (e.g., thousands of atoms), unlike some of the more accurate condensed matter methods. TB results can also be used as input to determine other properties (e.g., photoemission spectra) for which high accuracy is not essential.

B3.2.2.2 Applications of tight-binding methods

TB methods have been widely used to study properties of simple semiconductors such as Si [11] and GaN [16]. In the latter study, the effect of dislocations on the electronic structure of GaN was investigated with a view toward understanding how dislocations affect the material's optical properties. The large supercell of 224 atoms led to TB as the method of choice. This particular variant of TB fits TB matrix elements to DFT-LDA results and solves self-consistently for atomic charges. It has also been used to predict reaction energetics of organic molecules, the structure of large biomolecules and the surface geometry and band structure of III–V semiconductors [15]. The TB method is expected to provide qualitatively reasonable results for systems where localized atomic charges make sense and hence is not expected to perform as well for metallic systems. Despite potential problems of TB for metals, the TB approach has also been used to study the phonon spectrum of the transition metal molybdenum [6], the elastic constants, vacancies and surfaces of monatomic transition and noble metals and the Hall coefficient of complex perovskite crystals [10]. As an example of data available from a TB calculation, a TB variant of extended Hückel theory [21, 22] was used to describe the initial states in photoemission from GaN [23]. The parameters were fitted to the bulk band structure $E_n(k)$ (for a definition, see section A1.3.6). As displayed in figure B3.2.1, good agreement is found for the occupied states (negative energies), while larger differences for the conduction bands (positive energies) reveal a typical problem of the TB methods: they are far less capable of describing the delocalized conduction band states (the same is true for delocalized valence states in a metal, as mentioned above). In figure B3.2.2, we show a series of calculated photoemission spectra compared to experimental results [23]. The dispersion of the main peaks as a function of emission angle and photon energy agrees reasonably well in theory and experiment.

B3.2.3 First-principles electronic structure methods

In this section, we briefly review the basic elements of DFT and the LDA. We then focus on improvements suggested to remedy some of the shortcomings of the LDA (see section B3.2.3.1). A wide variety of techniques based on DFT have been developed to calculate the electron density. Many approaches do not calculate the density directly but rather solve for either a set of single-electron orbitals, or the Green's function, from which the density is derived.

In section B3.2.3.2, we introduce a number of techniques commonly referred to as *ab initio* all-electron electronic structure methods. *Ab initio* methods, in particular, aim at calculating the energies of electrons and their wavefunctions as accurately as possible, introducing as few adjustable parameters as possible. (Empirical or semi-empirical methods include the empirical pseudopotential approach (see section A1.3.5.5) and many TB techniques (see section B3.2.2).) Within the *ab initio* band structure approach, two communities exist that differ in their treatment of the singular nature of realistic, Coulomb-like crystal potentials. In the

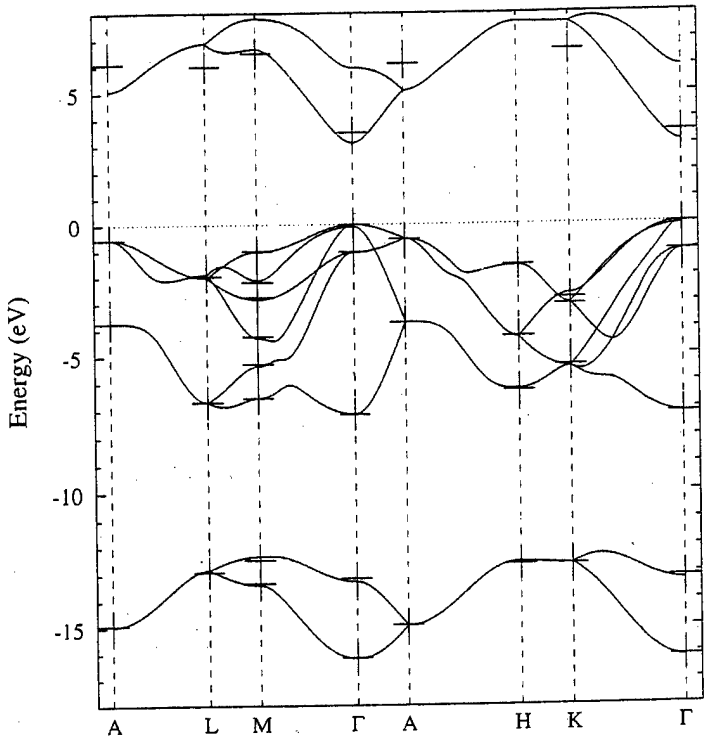

Figure B3.2.1. The band structure of hexagonal GaN, calculated using EHT-TB parameters determined by a genetic algorithm [23]. The target energies are indicated by crosses. The target band structure has been calculated with an *ab initio* pseudopotential method using a quasiparticle approach to include many-particle corrections [194].

pseudopotential approach discussed by Chelikowsky in chapter A1.3, the Coulomb singularity $(-Z/r)$ of the crystal potential is replaced by a smoother function, whereas in the so-called 'all-electron' approach, the Coulomb singularity is retained. The pseudopotential transformation limits the range of electron energies which can be accessed. However, since the pseudo-wavefunction is much smoother than the all-electron wavefunction (which has large oscillations near the nucleus), the pseudopotential allows the use of a plane wave basis set, which is comparatively easy to handle. In principle, the all-electron methods have no limitation on the energy range of calculations. This is achieved by a sophisticated representation of the wavefunction.

The so-called orbital-free DFT technique, which aims to directly calculate the electron density for which the total energy is minimal, is presented as an example of methods whose computational effort scales linearly with system size (see section B3.2.3.3). In section B3.2.3.4, we discuss the periodic HF method, an alternative approach to DFT that offers a well defined starting point for many-particle corrections. Finally, the two most frequently used QMC techniques are described in section B3.2.3.5.

B3.2.3.1 The local density approximation and beyond

In DFT, the electronic density rather than the wavefunction is the basic variable. Hohenberg and Kohn showed [24] that all the observable ground-state properties of a system of interacting electrons moving in an external potential $v_{\text{ext}}(r)$ are uniquely dependent on the charge density $\rho(r)$ that minimizes the system's total energy. However, there is no known formula to calculate from the density the total energy of many electrons moving in a general potential. Hohenberg and Kohn proved that there exists a universal functional of the density,

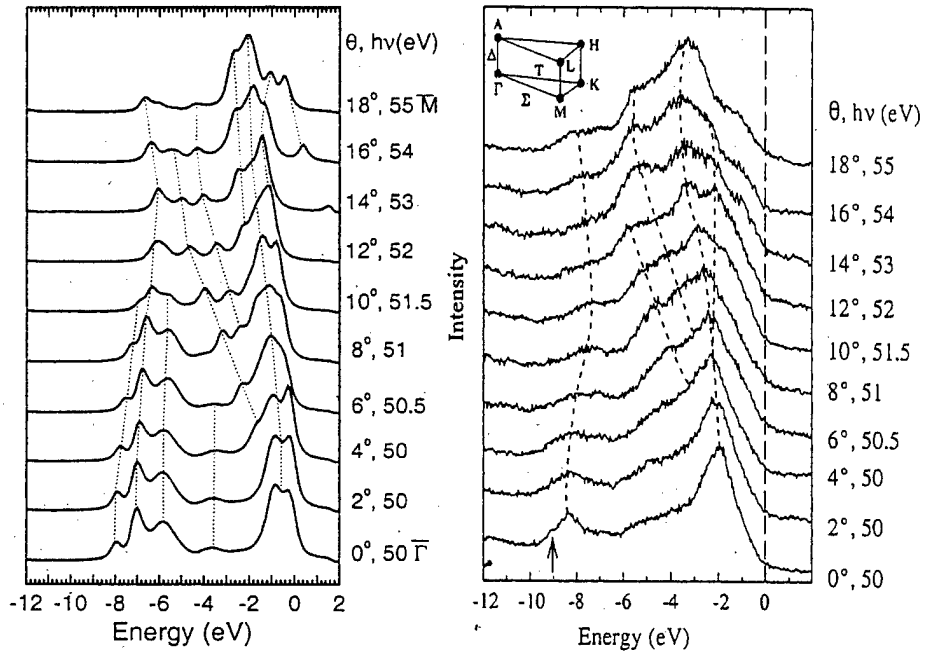

Figure B3.2.2. A series of photoemission spectra. The angles give the polar angle of electron emission at the stated photon energy scanning the surface Brillouin zone from $\bar{\Gamma}$ to $\bar{M}$. Left: A calculation using the tight-binding parametrization (given the band structure in figure B3.2.1) for the initial states [23]. Right: Experimental spectra by Dhesi *et al* [195]. The difference in binding energies is due to the experimental difficulty in determining the Fermi energy [23]. (Experimental figure by Professor K E Smith.)

called $G[\rho]$, such that the expression

$$E[\rho] = \int v_{\text{ext}}(r)\rho(r)\,\mathrm{d}^3r + \frac{1}{2}\int \frac{\rho(r)\rho(r')}{|r-r'|}\mathrm{d}^3r\,\mathrm{d}^3r' + G[\rho] \tag{B3.2.3}$$

has as its minimum value the correct ground-state energy associated with $v_{\text{ext}}(r)$. Here, the first term on the right-hand side represents the energy due to an external potential, including the electron–nuclear potential, while the second term is the classical Coulomb energy of the electronic system. The functional $G[\rho]$ is valid for any number of electrons and any external potential, but it is unknown and further steps are necessary to approximate it.

Kohn and Sham [25] decompose $G[\rho]$ into the kinetic energy of an analogous set of non-interacting electrons with the same density $\rho(r)$ as the interacting system,

$$T_{\text{s}}[\rho] = \sum_i \left\langle \psi_i \left| -\frac{1}{2}\nabla^2 \right| \psi_i \right\rangle$$

(where $\psi_i(r) \leftrightarrows \langle r|\psi_i\rangle$ is the wavefunction of electron i), and the exchange and correlation energy of an interacting system with density $\rho(r)$, $E_{\text{xc}}[\rho]$. The functional $E_{\text{xc}}[\rho]$ is not known exactly. Physically, it represents all the energy corrections beyond the Hartree term to the independent-particle model, i.e. the non-classical many-body effects of exchange and correlation (xc) and the difference between the kinetic energy of the interacting electron system $T[\rho]$ and the analogous non-interacting system $T_{\text{s}}[\rho]$.

In the LDA, the exchange and correlation energy is approximated using the exchange and correlation energy of the homogeneous electron gas at the same density (see section A1.3.3.3). The crystal density is obtained by solving the single-particle Kohn–Sham equation

$$\left(-\frac{1}{2}\nabla^2 + v_{\text{eff}}(r)\right)\psi_i(r) = E_i\psi_i(r), \tag{B3.2.4}$$

for a self-consistent potential v_{eff}, i.e. a potential which is produced by the density ρ. In bulk crystal calculations, the index i runs over both the Bloch vector k (see section A1.3.4) and the band index n (in a simple crystal, this band could be derived, for example, entirely from s states). The solutions to equation (B3.2.4) are often called Kohn–Sham orbitals. The crystal density is then

$$\rho(r) = \sum_i \psi_i^*(r)\psi_i(r).$$

The eigenenergy E_i can be defined as the derivative of the total energy of the many-electron system with respect to the occupation number of a specific orbital [26]. In HF theory (where equation (B3.2.4) applies and the v_{eff} contains a non-local exchange operator, see section A1.3.1.2 and chapter B3.1), Koopmans' theorem states that the single-particle eigenvalue is the negative of the ionization energy (neglecting the relaxation of the electronic system). In contrast, the identification of the highest occupied Kohn–Sham eigenvalue with the negative of the ionization energy is a controversial subject [27]. While there is no rigorous connection between eigenvalue differences and excitation energies in either HF or DF theory, comparisons of these values are common practice (see below for more appropriate methods). Relative differences among occupied single-particle energies often agree well with the experiment. Even though DFT only provides a solution for the ground state of the electronic system, the energy differences in the lower conduction bands, i.e. low-energy excited states, often are represented surprisingly well, too. However, in LDA calculations of semiconductors and insulators, almost always the size of the gap between the valence band maximum and the conduction band minimum is underestimated, since many-particle effects are incorrectly represented by the parametrized exchange-correlation energy (see, for example, [28]). One *ad hoc* remedy, which works well for many systems and which is employed in the examples presented here, is to use what is amusingly referred to as a *scissor operator*, i.e. a rigid shift, to correct the gap size [29, 30]. Typically the shift is determined by knowing, for example, the DFT error in predicting the measured optical band gap. The entire conduction band is shifted rigidly upward by the amount to match the experimental band gap.

More advanced techniques take into account quasiparticle corrections to the DFT-LDA eigenvalues. Quasiparticles are a way of conceptualizing the elementary excitations in electronic systems. They can be determined in band structure calculations that properly include the effects of exchange and correlation. In the LDA, these effects are modelled by the exchange–correlation potential $v_{\text{xc}}^{\text{LDA}}$. In order to more accurately account for the interaction between a particle and the rest of the system, the notion of a local potential has to be generalized and a non-local, complex and energy-dependent exchange–correlation potential has to be introduced, referred to as the self-energy operator $\Sigma(r, r'; E)$. The self-energy can be expanded in terms of the screened Coulomb potential W, where $W = \epsilon^{-1}v$ is the Coulomb interaction v screened by the inverse dielectric function ϵ^{-1}. In a lowest order expansion in W, the self-energy can be approximated as $\Sigma = GW$, giving the GW approximation [31]. Here G is the one-electron Green's function describing the propagation of an additional electron injected into a system of other electrons (it can also describe the extraction of an electron).

To be a bit more explicit (following [32, 33]), the quasiparticle energies and wavefunctions are given by

$$(T + v_{\text{ext}} + v_{\text{H}})\psi_{nk}(r) + \int \mathrm{d}r'\Sigma(r, r'; E_{nk})\psi_{nk}(r') = E_{nk}\psi_{nk}(r),$$

where T is the kinetic energy operator, v_{ext} is the external potential due to the ions, and v_H is the Hartree Coulomb interaction. Since the self-energy operator in general is non-Hermitian, the quasiparticle energies E_{nk} are complex in general, and the imaginary part gives the lifetime of the quasiparticle. To first order in W, the self-energy is then given by

$$\Sigma(r, r'; E) = \frac{i}{2\pi} \int d\omega e^{-i\delta\omega} G(r, r'; E - \omega) W(r, r'; \omega)$$

where δ is a positive infinitesimal and ω corresponds to an excitation frequency. The inputs are the full interacting Green's function,

$$G(r, r'; E) = \sum_{nk} \frac{\psi_{nk}(r)\psi^*_{nk}(r')}{E - E_{nk} - i\delta_{nk}},$$

where δ_{nk} is an infinitesimal and the dynamically screened Coulomb interaction,

$$W(r, r'; \omega) = \Omega^{-1} \int dr'' \epsilon^{-1}(r, r''; \omega) v(r'' - r'),$$

where ϵ^{-1} is the inverse dielectric matrix, $v(r) = 1/|r|$ and Ω is the volume of the system. Usually the calculations start with the construction of the Green's function and the screened Coulomb potential from self-consistent LDA results. The self-energy Σ then has to be obtained together with G in a self-consistent procedure. However, due to the severe computational cost of this procedure, it is usually not carried out (see, for example, [34]). Instead, it is common practice to construct the self-energy operator non-self-consistently using the self-consistent LDA results to determine quasiparticle corrections to the LDA energies, resulting in the quasiparticle band structure. The GW approximation has been applied to a wide range of metals, semiconductors and insulators, where it has been found to lead to striking improvements in the agreement of optical excitation spectra with the experiment (see, for example [32, 35–37]). Recent studies also found that the GW charge density is close to the experiment for diamond structure semiconductors [38], and lifetimes of low-energy electrons in metals have been calculated [39].

Another disadvantage of the LDA is that the Hartree Coulomb potential includes interactions of each electron with itself, and the spurious term is not cancelled exactly by the LDA self-exchange energy, in contrast to the HF method (see A1.3), where the self-interaction is cancelled exactly. Perdew and Zunger proposed methods to evaluate the self-interaction correction (SIC) for any energy density functional [40]. However, full SIC calculations for solids are extremely complicated (see, for example [41–43]). As an alternative to the very expensive GW calculations, Pollmann *et al* have developed a pseudopotential built with self-interaction and relaxation corrections (SIRC) [44]. The pseudopotential is derived from an all-electron SIC-LDA atomic potential. The relaxation correction takes into account the relaxation of the electronic system upon the excitation of an electron [44]. The authors speculate that '...the ability of the SIRC potential to produce considerably better band structures than DFT-LDA may reflect an extra nonlocality in the SIRC pseudopotential, related to the nonlocality or orbital dependence in the SIC all-electron potential. In addition, it may mimic some of the energy and the non-local space dependence of the self-energy operator occurring in the GW approximation of the electronic many body problem' [45].

The LDA also fails for strongly correlated electronic systems. Examples of such systems are the late 3d transition-metal mono-oxides MnO, FeO, CoO, and NiO. Within the local spin density approximation (LSDA), the energy gaps calculated for MnO and NiO are too small [46] and, even worse, FeO and CoO are predicted to be metallic, whereas experimentally they have been found to be large-gap insulators. While the GW approximation yields an energy gap of NiO in reasonable agreement with experiment [47], the computational cost of this procedure is very high. The SIC-LDA method reproduces quite well the strong localization of the d electrons in transition metal compounds, but the orbital energies obtained by SIC are usually in strong disagreement with experimental results (for transition metal oxides, for example, occupied

d bands are approximately $\frac{1}{2}$ Hartree below the oxygen valence band—a separation not seen in spectroscopic data: see, for example, the experimental results in [48]) [49]. An alternative solution to this problem is offered by the LDA+U method [49, 50], where LDA encompasses the LSDA. In the LDA+U technique, the electrons are divided into two subsystems which are treated separately: the strongly localized (d or f) electrons and the delocalized s and p electrons. The latter are treated by standard LDA. The on-site interactions among the strongly localized electrons on each atom, however, are taken into account by a term $\frac{1}{2}U\sum_{i\neq j} n_i n_j$, where n_i are the occupation numbers of the strongly localized orbitals and U is the Coulomb interaction parameter (for details on the first-principles calculation of U, see [51]). At least for localized d or f states, the LDA+U technique may be viewed as an approximation to the GW approximation [49]. Band gaps, valence band widths and magnetic moments have been calculated with LDA+U that agree with experiment for a variety of transition metal compounds [49, 52], among other applications.

B3.2.3.2 All-electron DFT methods

(a) Introduction

When the highest accuracy is sought for the electronic and geometric properties of crystals, all the electrons of the atoms in the crystal and the full Coulomb singularity of the nuclear potential must be accounted for. All-electron approaches, which do just that, generally cannot compete with pseudopotential techniques in speed and simplicity of algorithm. However, the latter suffer from severe drawbacks when it comes to the construction of the very pseudopotentials these methods depend upon: even for so-called *ab initio* potentials, the pseudopotentials are far from uniquely determined. Additionally, problems with transferability and the construction of potentials for such elements as the transition metals remain. All-electron techniques can deal with any element and there are no worries about transferability of the potential. However, the accuracy comes at a price: due to the Coulomb singularity of the potential at the nuclear positions, the wavefunctions are highly oscillatory close to the nucleus. For those all-electron methods that use wavefunctions to represent the electrons (a Green's function method, for example, does not), this means that a simple plane wave basis set cannot be used for the expansion of the wavefunctions. To reach convergence of a plane wave $\exp(\mathrm{i}\boldsymbol{k}\cdot\boldsymbol{r})$ expansion would require a prohibitive number of basis functions. Thus, specialized basis sets have been invented for all-electron calculations.

We now discuss the most important theoretical methods developed thus far: the augmented plane wave (APW) and the Korringa–Kohn–Rostoker (KKR) methods, as well as the linear methods (linear APW (LAPW), the linear muffin-tin orbital [LMTO] and the projector-augmented wave [PAW]) methods.

In the early all-electron techniques, the crystal was separated into spheres around the atoms, so-called 'muffin-tin' spheres, and the interstitial region in between. Inside the spheres, the potential was approximated as spherically symmetric, while in the interstitial region it was assumed to be constant. This shape approximation of the potential is reasonable for close-packed crystals such as hexagonally close-packed metals, where the spheres cover a large fraction of the crystal volume. However, in less densely arranged crystals, such as diamond structure semiconductors (see figure A1.3.4), the muffin-tin approximation leads to large errors. In the diamond and the related zincblende structures, only 34% of the volume is covered by touching muffin-tin spheres (figure B3.2.3). For all of the all-electron methods, versions have been developed that are not restricted to shape approximations of the potential. These techniques are referred to as general, or full, potential methods.

(b) The augmented plane wave method

The APW technique was proposed by Slater in 1937 [53, 54]. It remains the most accurate of the band structure methods for the muffin-tin approximation of the potential. The wavefunction is expanded in basis functions $\varphi_i(\boldsymbol{k}+\boldsymbol{G}_i, E, \boldsymbol{r})$, the APWs, each of which is identical to the plane wave $\exp(\mathrm{i}(\boldsymbol{k}+\boldsymbol{G}_i)\cdot\boldsymbol{r})$ in the interstitial

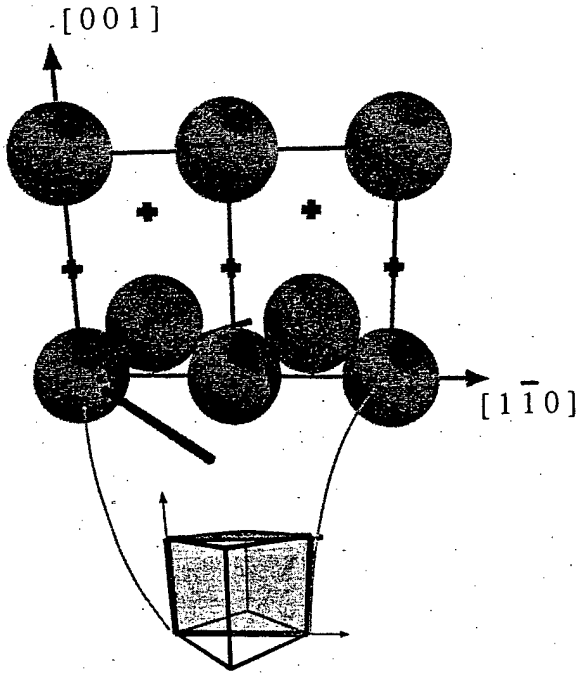

Figure B3.2.3. The muffin-tin spheres in the (110) plane of a zincblende crystal. The nuclei are surrounded by spheres of equal size, covering about 34% of the crystal volume. Unoccupied tetrahedral positions are indicated by crosses. The conventional unit cell is shown at the bottom; the crystal directions are noted.

region, where G_i are the reciprocal lattice vectors (see section A1.3.4). The plane waves are augmented, i.e. they are joined continuously at the surface of the spheres by solutions of the radial Schrödinger equation. This means that in the spherical harmonic expansion of a plane wave around the centre of a muffin-tin sphere, the respective Bessel function inside the sphere is replaced by a solution $\phi_{li}(r, E)$ of the radial Schrödinger equation for a given energy. The radial function matches the Bessel function, $j_l(|k + G_i|r)$, value at the sphere boundary and must be regular (non-singular) at the origin. With the basis functions $\varphi_i(k + G_i, E, r)$, a variational solution is sought to the Kohn–Sham equation, equation (B3.2.4). Since the Hamiltonian matrix elements now depend nonlinearly upon the energy due to the energy-dependent basis functions, the resulting secular equation is solved by finding the roots of the determinant of the $\underline{H}(E) - E\underline{S}(E)$ matrix. (The problem cannot be treated by the eigenvalue routines of linear algebra.)

Numerically, the determination of the roots can be difficult because the determinant's value may change by several orders of magnitude when the energy E is changed by only a few meV. Another difficulty can result at degenerate roots where the value of the determinant does not change sign. Additionally, the secular equation becomes singular when a node of the radial solution falls at the muffin-tin sphere boundary (the so-called 'asymptote problem').

Physically, the APW basis functions are problematic as they are not smooth at the sphere boundary, i.e., they have discontinuous slope. While in a fully converged solution of the secular equation, this discontinuity should disappear, alternative methods have been sought instead. Following a suggestion by Marcus [55] in 1967, the LAPW provided a way to avoid the above-mentioned drawbacks of the APW technique, as we now discuss.

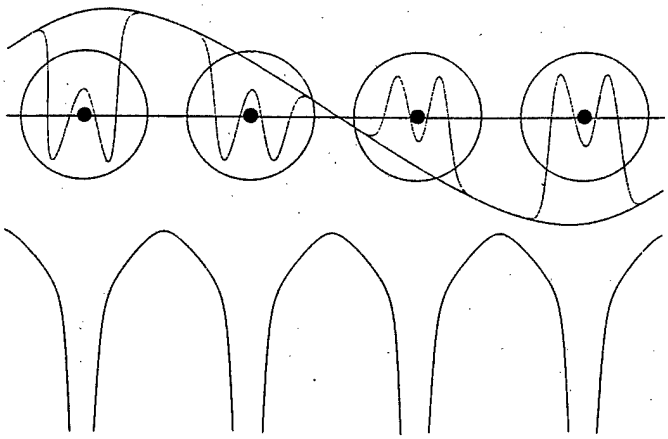

Figure B3.2.4. A schematic illustration of an energy-independent augmented plane wave basis function used in the LAPW method. The black sine function represents the plane wave, the localized oscillations represent the augmentation of the function inside the atomic spheres used for the solution of the Schrödinger equation. The nuclei are represented by filled black circles. In the lower part of the picture, the crystal potential is sketched.

(c) The linear augmented plane wave method

The main disadvantage of the APW technique is that it leads to a nonlinear secular problem because the basis functions depend on the energy. A number of attempts have been made to construct linear versions of the APW approach by introducing energy-independent basis functions in different ways. In 1970, Koelling invented the *alternative* APW [56] and Bross the *modified* APW [57]. In 1975, Andersen constructed the LAPW [58] formalism, which today is the most popular APW-like band structure method. Further extensions of the linear methods appeared in the early 1990s: Singh developed the LAPW *plus localized orbitals* (LAPW+LO [59]) in 1991 and Krasovskii the *extended* LAPW (ELAPW [60]) in 1994. Recently the APW+LO technique has been implemented by Sjöstedt and Nordström [61] according to an idea by Singh. While the LAPW technique is generally used in combination with DFT approaches, it has also been applied based on the LDA+U [62] and HF theories [63].

The LAPW method, as suggested in 1975 [58, 64], avoids the problem of the energy dependence of the Hamiltonian matrix by introducing energy-independent APW basis functions. Here, too, the APWs are derived from plane waves by augmentation: Bessel functions $j_l(|\boldsymbol{k}+\boldsymbol{G}_i|r)$ in the Rayleigh decomposition inside the muffin-tin sphere are replaced by functions $u_{li}(r)$ derived from the spherical potential, which are *independent* of the energy of the state that is sought and that match the Bessel functions at the sphere radius in value and in slope (see figure B3.2.4). The plane wave part of the basis remains the same but the energy-independent APWs allow the energies and the wavefunctions to be determined by solving a standard generalized eigenvalue problem.

In linearizing the APW problem as it is done in the LAPW method, the variational freedom of the APW basis set is reduced. The reason is that the wavefunction inside the spheres is rigidly coupled to its plane wave expansion in the interstitial region [65]. This means that the method cannot yield an accurate wavefunction even if the eigenvalue is within a few eV of the chosen energy parameters [66]. Flexibility is defined in this context as the possibility to change the wavefunction inside the spheres independently from the wavefunction in the interstitial region. Flexibility can be achieved in the linear band structure methods by adding basis functions localized inside the spheres whose value and slope vanish at the sphere boundary [54, 67, 68]. A 'flexible' basis set extending the LAPW with localized functions is preferable to the one used in the pure

LAPW technique. Flexible linear methods are the MAPW, the LAPW+LO and the ELAPW, the latter of which provides a necessary degree of flexibility with a minimal number of basis functions [65].

The additional functions increase the matrix dimension slightly and thus the computational effort. However, the increased flexibility of the basis set makes possible a number of extensions of the LAPW method. One is a $k \cdot p$ formulation of the ELAPW method [68], which would lead to large errors in the regular LAPW due to its lesser flexibility. The augmented Fourier components (AFC) technique [69] for treating a general potential is based on this. The AFC method is an alternative to the full-potential LAPW (FLAPW) method [70, 71]. (Recently progress has been made in increasing the computational efficiency of the FLAPW method [72].) The AFC method does not have the same demanding convergence criteria as the FLAPW method but yields physically equivalent results [69].

The general potential LAPW techniques are generally acknowledged to represent the state of the art with respect to accuracy in condensed matter electronic-structure calculations (see, for example, [62, 73]). These methods can provide the best possible answer within DFT with regard to energies and wavefunctions.

(d) The Korringa–Kohn–Rostoker technique

The KKR method uses multiple-scattering theory to solve the Kohn–Sham equations [74, 75]. Rather than calculate the wavefunction, modern incarnations calculate the Green's function G. The Green's function is the solution to the equation schematically given by $(H - E)G(E) = -\delta$, where H is the Hamiltonian, E the single-electron energy and δ the delta function $\delta(r - r')$. The properties of the system, such as the electron density, the density of states and the total energy can be derived from the Green's function [73]. The crystal is represented as a sum of non-overlapping potentials; in the modern version, there are no shape approximations, i.e. the potentials are space-filling [76]. Within the multiple-scattering formalism, the wavefunction is built up by taking into account the scattering and rescattering of a free-electron wavefunction by scatterers. The scatterers are (generally) the atoms of the crystal and the single-scattering properties (the properties of the isolated scatterer) are derived from the effective, singular potentials of the atoms (given in equation (B3.2.2)). The Green's matrix is then constructed from the knowledge of the scattering properties of the single scatterers and the analytically known Green's function of the free electron. The full-potential KKR method has been shown to have the same level of accuracy as the full-potential LAPW method [73]. The Green's function formulation offers the advantage of easy inclusion of defects in the bulk or clean surfaces. Such calculations start with the Green's function of the periodic crystal and include the perturbation through a Dyson equation [77]. Yussouff states that the difference in speeds between the linear methods and his 'fast' KKR technique is at most a factor of ten, in favour of the former [78]. While the KKR technique has an accuracy comparable to the APW method, it has the disadvantage of not being a linear approach, limiting speed and simplicity.

(e) The linear muffin-tin orbital method

The LMTO method [58, 79] can be considered to be the linear version of the KKR technique. According to official LMTO historians, the method has now reached its 'third generation' [79]: the first starting with Andersen in 1975 [58], the second commonly known as TB-LMTO. In the LMTO approach, the wavefunction is expanded in a basis of so-called muffin-tin orbitals. These orbitals are adapted to the potential by constructing them from solutions of the radial Schrödinger equation so as to form a minimal basis set. Interstitial properties are represented by Hankel functions, which means that, in contrast to the LAPW technique, the orbitals are localized in real space. The small basis set makes the method fast computationally, yet at the same time it restricts the accuracy. The localization of the basis functions diminishes the quality of the description of the wavefunction in the interstitial region.

In the commonly used atomic sphere approximation (ASA) [79], the density and the potential of the crystal are approximated as spherically symmetric within overlapping muffin-tin spheres. Additionally, all

integrals, such as for the Coulomb potential, are performed only over the spheres. The limits on the accuracy of the method imposed by the ASA can be overcome with the full-potential version of the LMTO (FP-LMTO) which gives highly accurate total energies [79, 80]. It was found that the FP-LMTO is 'at least as accurate as, and much faster than,' pseudopotential plane wave calculations in the determination of structural and dynamic properties of silicon [80]. The FP-LMTO is considerably slower than LMTO-ASA, however, and it has been found that ASA calculations can yield accurate results if the full expansion, rather than only the spherical part, of the charge is used in what is called a full-charge (rather than a full-potential) method and the integrals are performed exactly [73, 79].

The LMTO method is the fastest among the all-electron methods mentioned here due to the small basis size. The accuracy of the general potential technique can be high, but LAPW results remain the 'gold standard'.

(f) The projector augmented wave technique

The projector augmented-wave (PAW) DFT method was invented by Blöchl to generalize both the pseudopotential and the LAPW DFT techniques [81]. PAW, however, provides all-electron one-particle wavefunctions not accessible with the pseudopotential approach. The central idea of the PAW is to express the all-electron quantities in terms of a pseudo-wavefunction (easily expanded in plane waves) term that describes interstitial contributions well, and one-centre corrections expanded in terms of atom-centred functions, that allow for the recovery of the all-electron quantities. The LAPW method is a special case of the PAW method and the pseudopotential formalism is obtained by an approximation. Comparisons of the PAW method to other all-electron methods show an accuracy similar to the FLAPW results and an efficiency comparable to plane wave pseudopotential calculations [82, 83]. PAW is also formulated to carry out DFT dynamics, where the forces on nuclei and wavefunctions are calculated from the PAW wavefunctions. (Another all-electron DFT molecular dynamics technique using a mixed-basis approach is applied in [84].)

PAW is a recent addition to the all-electron electronic structure methods whose accuracy appears to be similar to that of the general potential LAPW approach. The implementation of the molecular dynamics formalism enables easy structure optimization in this method.

(g) Illustrative examples of the electronic and optical properties of modern materials

As an indication of the types of information gleaned from all-electron methods, we focus on one recent approach, the ELAPW method. It has been used to determine the band structure and optical properties over a wide energy range for a variety of crystal structures and chemical compositions ranging from elementary metals [60] to complex oxides [85], layered dichalcogenides [86, 87] and nanoporous semiconductors [88]. The $\boldsymbol{k} \cdot \boldsymbol{p}$ formulation has also enabled calculation of the complex band structure of the Al (100) surface [89].

As an illustration of the accuracy of the AFC ELAPW-$\boldsymbol{k} \cdot \boldsymbol{p}$ method, we present the dielectric function of GaAs. The dielectric function is a good gauge of the quality of a method, since not only do the energies enter the calculation, but also the wavefunctions *via* the matrix elements of the momentum operator $-i\nabla$. For the calculation of the dielectric function (equation (A1,3.87)) of GaAs, the conduction bands were rigidly shifted so that the highest peak agreed in both experiment and theory, a shift of 0.75 eV. The imaginary part of the dielectric function is shown in figure B3.2.5. Comparing the energy differences between the three peaks, we find that they agree to within 2 meV. For a wider comparison, we plot the results of two more experiments (which only have measured the two peaks at lower photon energy) and several all-electron calculations of the dielectric function of GaAs in figure B3.2.6. The FLAPW results agree almost exactly with the AFC ELAPW values. The discrepancies compared to the experimental results found for the other methods are considerably larger than for the general potential LAPW results, particularly for E_1.

A recent study of a class of nanoporous materials, the cetineites [88], offers further illustration of the possibilities offered by the modern band structure methods. The crystal is constructed of tubes of 0.7 nm

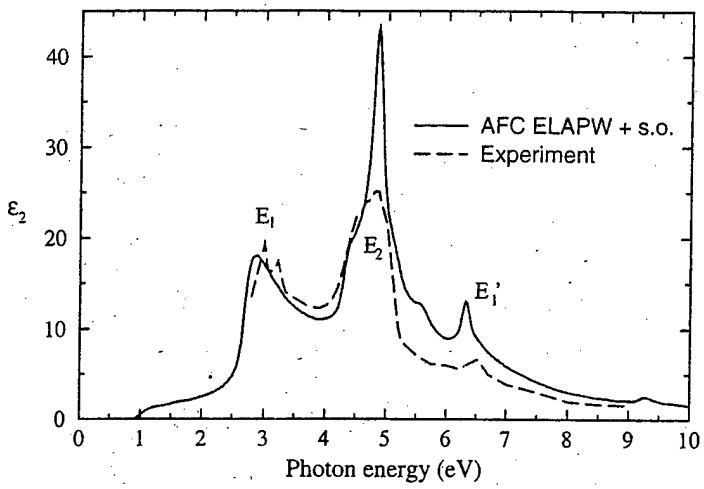

Figure B3.2.5. The imaginary part of the dielectric function of GaAs, according to the AFC ELAPW-$k \cdot p$ method (solid curve) [195] and the experiment (dashed curve) [196]. To correct for the band gap underestimated by the local density approximation, the conduction bands have been shifted so that the E_2 peaks agree in theory and experiment.

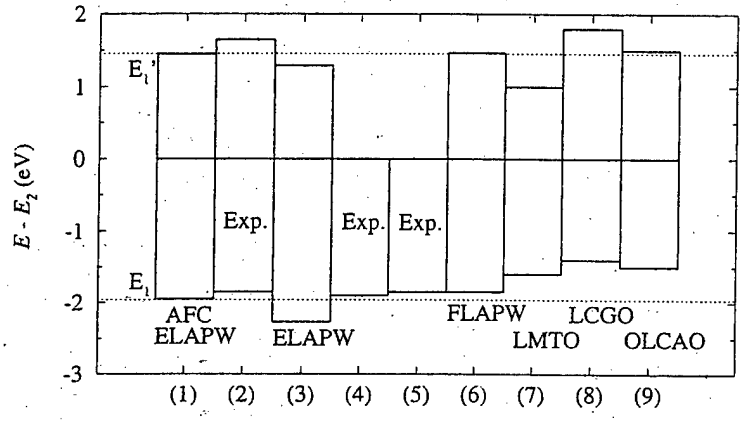

Figure B3.2.6. The energies of the E_1 and E_1' peaks relative to the E_2 peak of the imaginary part of the dielectric function of GaAs, calculated by self-consistent DFT all-electron methods. These energies do not depend on the gap size. The theoretical methods are noted, as are experimental results obtained by ellipsometry (see chapter B1.26). The lower (upper) histogram gives the energy of peak E_1 (E_1') relative to E_2. LCGO designates a linear-combination-of-Gaussian-orbitals method, OLCAO an orthogonalized linear-combination-of-atomic-orbitals approach. Sources: (1) [195], (2) [196], (3) [197], (4) [198], (5) [199], (6) [200], (7) [199], (8) [201], (9) [202].

diameter arranged in a two-dimensional hexagonal structure with 'flattened' $SbSe_3$ pyramids arranged between the tubes (see figure B3.2.7). Cetineites are of potential technological interest because, singularly among nanoporous materials, they are semiconductors rather than insulators. In figure B3.2.8, we show the comparison of the predicted density of states to the ultraviolet photoemission spectrum (PES, see chapter B1.1). The DOS can explain the two main structures in the PES at about -3 and -12 eV. Their relative intensities agree with those suggested by the DOS curve. Three structures in the DOS at -1, -6 and -9 eV

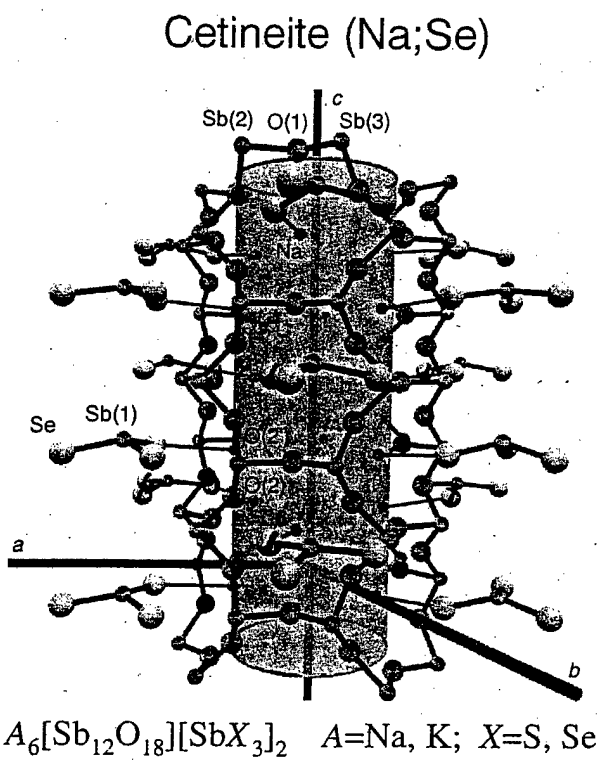

Figure B3.2.7. A perspective view of the cetineite (Na;Se). The height of the figure is three lattice constants *c*. The shaded tube is included only as a guide to the eye. (From [88].)

are not resolved in the PES. This may be due to the selection rules of the photoemission process, not accounted for in the theory, or perhaps due to incomplete angle integration experimentally. The experimental results confirm, in particular, that the number of states is very high close to the valence band maximum. An orbital analysis shows that these states are derived mainly from the p states of the O and Se constituents of the crystal, with the chalcogen dominating near the top of the valence band. Electrons in the Se p states are thus most easily excited into the conduction band. This, together with their high DOS, makes the Se p states located on the pyramids the prime candidates for the initial states of the photoconductivity observed in the cetineites.

As another example of properties extracted from all-electron methods, figure B3.2.9 shows the results of a PAW simulation of benzene molecules on a graphite surface. The study aimed to show the extent to which the electronic structure of the molecule is modified by interaction with the surface, and why the images do not reflect the molecular structure. The PAW method was used to determine the structure of the molecule at the surface, the strength of the interaction between the surface and the molecules, and to predict and explain scanning tunnelling microscope (STM) images of the molecule on the surface [90] (the STM is described in section B1.19).

B3.2.3.3 Linear-scaling electronic structure methods

DFT calculations such as the ones mentioned in chapter A1.3 and section B3.2.3.2 become computationally very expensive when the unit cell of the interesting system becomes large and complex, with certain parts of the computational algorithm typically scaling cubically with system size. A recent objective for treating large

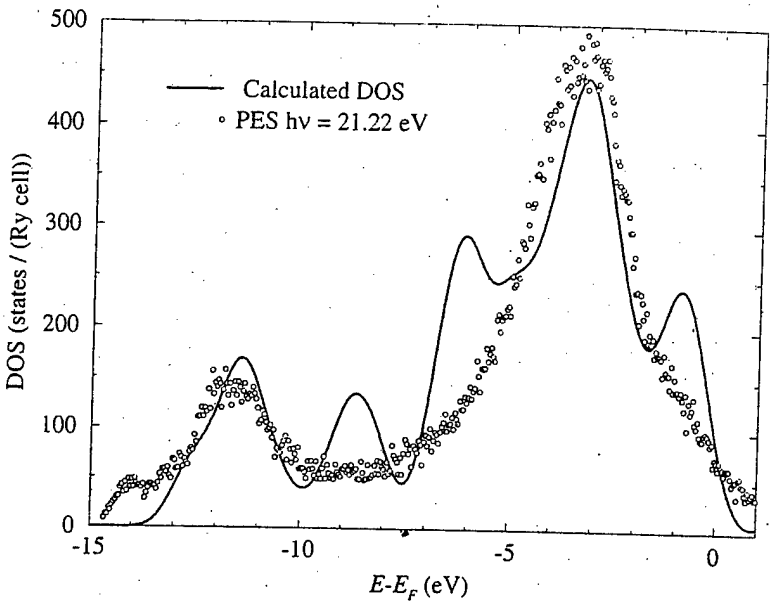

Figure B3.2.8. Comparison of the photoemission spectrum for the cetineite (Na;Se) and the density of states calculated by the AFC ELAPW-$k \cdot p$ method [88].

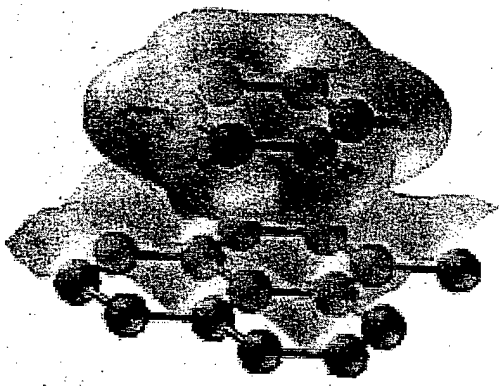

Figure B3.2.9. A benzene molecule on a graphite surface [90]. The geometry and the charge density (indicated by the surfaces of constant density) have been obtained using the PAW method. (Figure by Professor P E Blöchl.)

systems is to have the computational burden scale no more than linearly with system size. Methods achieving this are called linear-scaling or O(N) (order N) methods, most of which are based on the Kohn–Sham equation (see equation (B3.2.4)), aiming to calculate single-electron wavefunctions, the Kohn–Sham orbitals. These methods tend to be faster than the conventional Kohn–Sham approach above a few hundred atoms [20, 91–93]. Another class of methods is based directly on the DFT of Hohenberg and Kohn [24]. With these techniques one seeks to determine directly the density that minimizes the total energy; they are often referred to as orbital-free methods [94–97]. Such orbital-free calculations do not have the bottlenecks present in orbital-based O(N) DFT calculations, such as the need to localize orbitals to achieve linear scaling, orbital orthonormalization, or Brillouin zone sampling. Without such bottlenecks, the calculations become very inexpensive.

Equation (B3.2.3) lists the terms comprising the calculation of the total energy. The term due to the external potential and the Hartree term describing the Coulomb repulsion energy among the electrons already explicitly depend on the density instead of on orbitals. More difficult to evaluate is $G[\rho] = T_s[\rho] + E_{xc}[\rho]$, a functional which is not known exactly. However, over the years a number of high-quality exchange–correlation functionals have been developed for all kinds of systems. Only quite recently have more accurate kinetic energy density functionals (KEDFs) become available [97–99] that afford linear-scaling computations.

One current limitation of orbital-free DFT is that since only the total density is calculated, there is no way to identify contributions from electronic states of a certain angular momentum character l. This identification is exploited in non-local pseudopotentials so that electrons of different l character 'see' different potentials, considerably improving the quality of these pseudopotentials. The orbital-free methods thus are limited to local pseudopotentials, connecting the quality of their results to the quality of the available local potentials. Good local pseudopotentials are available for the alkali metals, the alkaline earth metals and aluminium [100, 101] and methods exist for obtaining them for other atoms (see section VI.2 of [97]).

The orbital-free method has been used for molecular-dynamics studies of the formation of the self-interstitial defect in Al [102], pressure-induced glass-to-crystal transitions in sodium [103] and ion–electron correlations in liquid metals [101]. Calculations of densities for various Al surfaces have shown excellent agreement between the charge densities as calculated by Kohn–Sham DFT and an orbital-free method using a KEDF with a density-dependent response kernel [99]. The method was used recently to examine the metal–insulator transition in a two-dimensional array of metal quantum dots [104], where the theory showed that minute overlap of the nanoparticle's wavefunctions is enough to transform the array from an insulator to a metal. As an example of the ease with which large simulations can be performed, figure B3.2.10 shows a plot of the charge density from an orbital-free calculation of a vacancy among 255 Al atoms [98], carried out on a workstation.

B3.2.3.4 The Hartree–Fock method in crystals

The HF method (discussed in section A1.3.1.2) is an alternative to DFT approaches. It does not include electron correlation effects, i.e. non-classical electron–electron interactions beyond the Coulomb and exchange interactions. The neglect of these terms means that the Coulomb interaction is unscreened, and hence the electron repulsion energy is too large, overestimating ionic character, which leads to band gaps that are too large by a factor of two or more and valence band widths that are too wide by 30–40% [63]. However, the HF results can be used as a well defined starting point for the inclusion of many-particle corrections such as the GW approximation [31, 32] or, with considerably less computational effort, the results can be improved considerably by accounting for the Coulomb hole and screening the exchange interaction using the dielectric function [63, 105].

Ab initio HF programs for crystals have been developed [106, 107] and have been applied to a wide variety of bulk and surface systems [108, 109]. As an example, a periodic HF calculation using pseudopotentials and an LCAO basis predicted binding energies, lattice parameters, bulk moduli and central-zone phonon frequencies of 17 III–V and IV–IV semiconductors. The authors find that '...[o]n the whole, the HF LCAO data appear no worse than other *ab initio* results obtained with DF-based Hamiltonians' [110]. They suggest that the largest part of the errors with respect to experiment is due to correlation effects and to a lesser extent due to the imperfections of the pseudopotentials [110]. More recently, the electronic and magnetic properties of transition metal oxides and halides such as perovskites, which had been a problem earlier, have been investigated with spin-unrestricted HF [111]. In general, the periodic HF method is best suited for the study of highly ionic, large band gap crystals because such systems are the least sensitive to the lack of electron correlation.

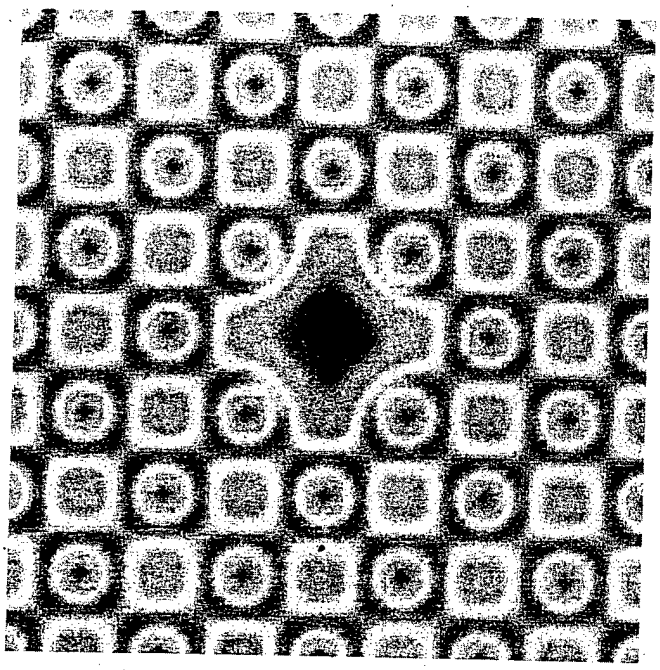

Figure B3.2.10. Contour plot of the electron density obtained by an orbital-free Hohenberg–Kohn technique [98]. The figure shows a vacancy in bulk aluminium in a 256-site cell containing 255 Al atoms and one empty site, the vacancy. Dark areas represent low electron density and light areas represent high electron density. A Kohn–Sham calculation for a cell of this size would be prohibitively expensive. Calculations on smaller cell sizes using both techniques yielded densities that were practically identical.

B3.2.3.5 Quantum Monte Carlo

QMC techniques provide highly accurate calculations of many-electron systems. In variational QMC (VMC) [112–114], the total energy of the many-electron system is calculated as the expectation value of the Hamiltonian. Parameters in a trial wavefunction are optimized so as to find the lowest-energy state (modern methods instead minimize the variance of the local energy $\frac{H\Psi}{\Psi}$ [115]). A Monte Carlo (MC) method is used to perform the multi-dimensional integrations necessary to determine the expectation value,

$$E = \frac{\int |\Psi|^2 \frac{H\Psi}{\Psi} \mathrm{d}\tau}{\int |\Psi|^2 \mathrm{d}\tau}$$

where Ψ is the trial wavefunction and $|\Psi|^2 / \int |\Psi|^2 \mathrm{d}\tau$ is a normalized probability distribution. The integration is performed by summing up the local energy at points, corresponding to electron configurations, given by the probability distribution. A random walk algorithm, such as the Metropolis algorithm [116], is used to sample those regions of configuration space more heavily where the probability density is high. The standard Slater–Jastrow trial wavefunction is the product of a Slater determinant of single-electron orbitals and a Jastrow factor, a function which includes the description of two-electron correlation. As an example, the trial wavefunction used for a silicon crystal contained 32 variational parameters whose optimization required the calculation of the local energy for 10 000–20 000 statistically independent electron configurations [117]. In contrast to the DMC technique described below, the accuracy of a VMC calculation depends on the quality of the many-particle wavefunction used [114]. In figure B3.2.11, we show the determination of the lattice

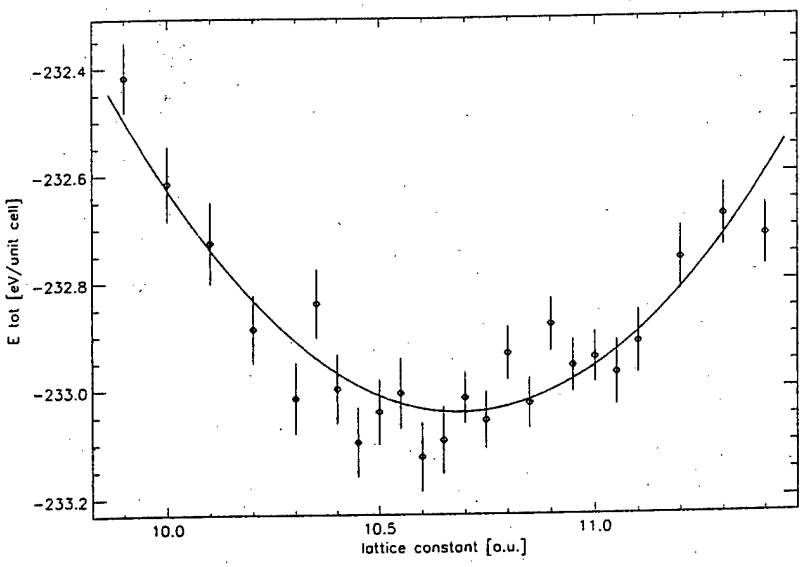

Figure B3.2.11. Total energy *versus* lattice constant of gallium arsenide from a VMC calculation including 256 valence electrons [118]; the curve is a quadratic fit. The error bars reflect the uncertainties of individual values. The experimental lattice constant is 10.68 au, the QMC result is 10.69 (±0.1) au (Figure by Professor W Schattke).

constant of GaAs by VMC by minimization of the total energy [118]. This figure illustrates the roughness of the potential energy surface due to statistical errors, which poses a challenge then for the calculation of forces with QMC.

In the diffusion QMC (DMC) method [114, 119], the evolution of a trial wavefunction (typically wavefunctions of the Slater–Jastrow type, for example, obtained by VMC) proceeds in imaginary time, $\tau = it$, according to the time-dependent Schrödinger equation, which then becomes a diffusion equation. All components of the wavefunction except for the ground-state wavefunction are damped by the time evolution operator $\exp(-iHt) = \exp(-H\tau)$. The DMC was developed as a simplification of the Green's function MC technique [113]. A particularly well known use of the Green's function MC technique was the determination by Ceperley and Alder of the energy of the uniform electron gas as a function of its density [120]. This $E(\rho)$ was subsequently parametrized by Perdew and Zunger for the commonly used LDA exchange–correlation potential [40]. Usually two approximations are made to make DMC calculations tractable: the fixed-node approximation, in which the nodes, the places where the trial function changes sign, are kept fixed for the solution to enforce the fermion symmetry of the wavefunction and the so-called short-time approximation, whose effect can be made very small [114]. Excited states have been calculated by replacing an orbital in the Slater determinant of the trial wavefunction by a conduction-band orbital [121].

Recently, a method has been proposed to overcome the problems associated with calculating forces in both VMC and DMC [122]. It has been suggested that the use of QMC in the near future to tackle the energetics of systems as challenging as liquid binary iron alloys is not unthinkable [123].

B3.2.3.6 Summary and comparisons

As we have outlined, a very wide variety of methods are available to calculate the electronic structure of solids. Empirical TB methods (such as discussed in section B3.2.2) are the least expensive, affording the calculation of unit cells with large numbers (e.g. 10^3) of atoms, or to provide cheap input to subsequent

methods, at the price of quantitative accuracy. DFT methods (sections A1.3.5.4 and B3.2.3.3), on the other hand, are responsible for many of the impressive results obtained in computational materials theory in recent years. The tradeoff for DFT is the opposite: its expense, except in the not-yet-general linear scaling methods, limits it typically to systems with at most a few hundred atoms. Once the O(N) DFT methods become more general (for example, when orbital-free DFT can treat non-metallic systems), then the DFT method will be able routinely to treat systems as large as those treated now with TB.

The diversity of approaches based on HF (section B3.2.3.4) is small at present compared to the diversity found for DFT. For solids, HF appears to yield results inferior to DFT due to the neglect of electron correlation, but being a genuine many-particle theory it offers the possibility for consistent corrections, in contrast to DFT. Finally, the QMC techniques (section B3.2.3.4) hold promise for genuine many-particle calculations, yet they are still far from able to offer the same quantities for the same range of materials and geometries as the theories mentioned before. With this wide range of methods now introduced, we will look at their application to chemisorption on solid surfaces.

B3.2.4 Quantum structural methods for solid surfaces

B3.2.4.1 Introduction

First-principles models of solid surfaces and adsorption and reaction of atoms and molecules on those surfaces range from *ab initio* quantum chemistry (HF; configuration interaction (CI), perturbation theory (PT), etc: for details see chapter B3.1) on small, finite clusters of atoms to HF or DFT on two-dimensionally infinite slabs. In between these two extremes lie embedded cluster models, which recognize and attempt to correct the drastic approximation made by using a finite cluster to describe, for example, a metallic conductor whose electronic structure is inherently delocalized or an ionic crystal with long-range Coulomb interactions. Upon chemisorption, the binding of an atom or a molecule to a surface involves significant sharing of electrons in the bond between the adsorbate and surface atoms and this breaking of the crystal symmetry will induce localization of the electrons. The attractive feature of the embedded cluster idea is that it preserves the strengths of the cluster approach, namely it allows one to describe the very local process of chemisorption to a high degree of accuracy by, for example, quantum chemical methods, while at the same time attempting to account for the presence of the rest of the surface and bulk. Surface reconstruction and molecular adsorption have been studied on a variety of surfaces, including insulators, semiconductors and metals. To illustrate these methods, we will focus on those used to examine adsorption of atoms and molecules on transition metal surfaces. This is not a comprehensive review of each approach; rather, we provide selected examples that demonstrate the range of techniques and applications, and some of the lessons learned.

B3.2.4.2 The finite cluster model

The most straightforward molecular quantum mechanical approach is to treat adsorption on a small, finite cluster of transition metal atoms, ranging from as small as four atoms up to ~40 atoms. Though all-electron calculations can be performed, typically the core electrons of transition metal atoms are replaced by an effective core potential (ECP, the quantum chemistry version of a pseudopotential that accounts approximately for the core–valence electron interaction), while the valence electrons of each metal atom are treated explicitly within a HF, CI, PT, or DFT formalism. Typically, a few atoms in the chemisorption region contain the valence (or all) electrons explicitly, while surrounding atoms tend to be described more crudely with, for example, a one-electron ECP representation, model pseudopotentials or, in the case of ionic crystals, a finite array of point charges. Generally, the structure of the cluster is chosen to be a fixed fragment of the bulk. Examples of this type of approach include the early work of Upton and Goddard [124], who examined adsorption of electronegative and electropositive atoms on a Ni_{20} cluster designed to mimic various low-index faces of Ni. In this model, only the 4s electrons on each Ni atom were treated explicitly, while the 3d electrons were

subsumed into an ECP. They made predictions concerning preferred binding sites, geometries, vibrational frequencies and binding energies. Bagus *et al* [125] published an important comparison study showing that it is more accurate to treat metal atoms directly interacting with an adsorbate at an all-electron level, while it is sufficient to describe the surrounding metal atoms with ECPs. Panas *et al* [126] proposed the idea that a cluster should be 'bond-prepared', namely that one should study an electronic state of the finite cluster that has enough singly-occupied orbitals of the correct symmetry to interact with the incoming admolecule to form the necessary covalent bonds between the adsorbate and the metal. In one of the first studies of a metal surface reaction, Panas *et al* [127] examined dissociative chemisorption pathways at the multi-reference CI level for O_2 on a Ni_{13} cluster, generally using ECPs for all but the 4s electrons. Salahub and co-workers [128] used DFT-LDA with a Gaussian basis to examine chemisorption of C, O, H, CO and HCOO on Ni clusters containing up to 16 atoms meant to represent various low-index faces of Ni. Gradient corrections to the LDA scheme improved dramatically the binding energies for hydrogen bound to small Ni clusters, when compared to experimental results for Ni(111) and Ni(100) [129]. Multiple adsorbates were also studied by DFT-LDA: for example, in the case of hydrogen on Pd clusters modelling Pd(110) [130]. Diffusion barriers were also calculated by DFT-LDA for clusters containing up to 13 metal atoms of Pd, Rh, Sn, and Zn [131]. Other examples include HF calculations of K adsorbed on Cu clusters [132], HF and Møller–Plesset second-order PT (MP2) calculations of acetylene on Cu and Pd clusters [133], modified coupled pair functional (CPF) calculations for CO on Cu clusters [134], averaged CPF calculations of hydrogen adsorption on relaxed Cu clusters [135], HF, CASSCF (complete active space self-consistent field) and multireference CI and PT calculations for CO [136] and O [137] on Pt clusters, and spin-polarized DFT of c-CH_2N_2 on Pd and Cu tetramers [138] and of K and CO on $Pd_{8,14}$ [139]. The advantage of the finite-cluster model is that one can systematically include high levels of electron correlation; this is to be balanced against the lack of a proper band structure, the presence of edge effects and the fact that it is generally limited to modelling low coverages. Next we outline current strategies for ameliorating some of these difficulties.

B3.2.4.3 Finite-cluster model in contact with a classical background

Several modifications of the finite-cluster model meant to account for the background Fermi sea of electrons and to compensate for the lack of a proper band structure have been developed. They rely on simple approximations of the surface/bulk, usually involving classical electrostatic interactions and usually applied to ionic crystals (see, for example, [140]). Of these, the model invented by Nakatsuji is the primary one that has considered adsorption on metal surfaces [141]. The so-called 'dipped adcluster model' [142] considers a small cluster plus an adsorbate as the 'adcluster' that is 'dipped' onto the Fermi sea of electrons of the bulk metal. A normal HF calculation on the small system is performed, in which electrons are added to or removed from the cluster in each calculation. By comparing the variation in the total energy with respect to the fractional electron transfer, dE/dn, to the work function of the metal, μ, the extent of electron transfer between the adcluster and the bulk metal can be established. Thus, charges on a small cluster are optimized and an image charge correction is also accounted for. In certain cases, integral charges are transferred between the cluster and the 'surroundings'; then electron correlation calculations, for example CI, can be carried out. This is a purely classical electrostatic approach to accounting for the background electrons in an implicit, rather than explicit, manner. Nakatsuji has used this to study adsorption of ionic adsorbates on metals, and finds that one can describe the polarization of the metal reasonably well. We have worked briefly with this approach [143], but found that there is a problem with extending the method beyond two-dimensional clusters, because of an ambiguity of where to place the image plane. Indeed, Nakatsuji's examples are always small one- or two-dimensional clusters. It is also likely that the wavefunction for such small clusters (typically $\leq$4 metal atoms) would not adequately represent a true metal surface wavefunction.

A simple, implicit means of describing the metallic band structure [144] was introduced by Rösch, using a Gaussian broadening of the cluster energy levels in order to determine a cluster Fermi level within DFT,

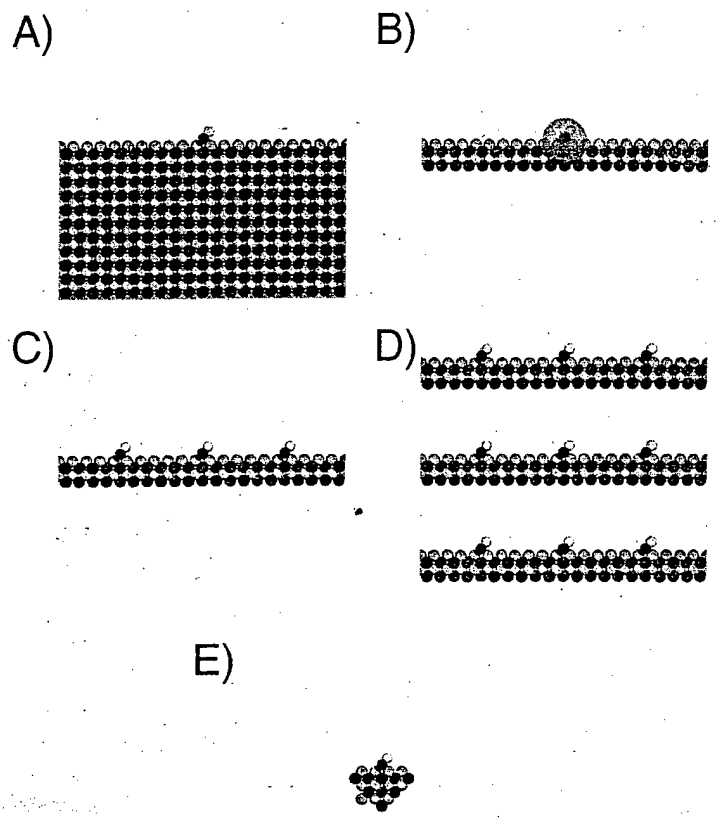

Figure B3.2.12. Schematic illustration of geometries used in the simulation of the chemisorption of a diatomic molecule on a surface (the third dimension is suppressed). The molecule is shown on a surface simulated by (A) a semi-infinite crystal, (B) a slab and an embedding region, (C) a slab with two-dimensional periodicity, (D) a slab in a supercell geometry and (E) a cluster.

originally by the X_α method (a simplified version of DFT-LDA; see section A1.3.3.3). Recent applications of this method have utilized more accurate forms of gradient-corrected spin-polarized DFT to look at adsorption of, for example, acetylene on $Ni_{14,20}$ clusters [145], CO adsorption on Ni, Pd and Pt clusters of eight or nine atoms [146] and NO adsorption on Ru [147].

B3.2.4.4 Slab calculations

The other extreme of modelling chemisorption is to use a slab described by DFT or HF. The slab is typically taken to be periodic in the directions parallel to the surface and contains a few atomic layers in the direction normal to the surface. For the adatoms not to influence each other, unless that is intended, the unit cell needs to be sufficiently large, parallel to the surface. For computational reasons, it is advantageous in some methods, namely plane wave techniques, to have periodicity in three dimensions. In the supercell geometry, this periodicity is gained by considering slabs which are periodic in the direction perpendicular to the surface

but separated from each other by vacuum regions. The vacuum region has to be thick enough so that there is no influence between the surfaces facing each other (the same is true for the slab thickness). For a schematic description of several simulation model geometries, see figure B3.2.12.

Freeman and co-workers developed the FLAPW method (see B3.2.2) during the early 1980s [70, 148]. This was a major advance, because the conventional 'muffin-tin' potential was eliminated from their calculation allowing general-shape potentials to be evaluated instead. Freeman's group first developed this for thin films and then for bulk metals. As mentioned before, the LAPW basis, along with the elimination of any shape approximations in the potential, allows for highly accurate calculations on transition metal surfaces, within the DFT-LDA and the generalized gradient approximation, GGA (see section A1.3.3.3). For the 'stand-alone' slab geometry, figure B3.2.12(C), the LAPW basis functions decay exponentially into the vacuum. The numerous interfacial systems examined by Freeman's group include, for example, CO with K or S coadsorption on Ni(001) [149], adsorption of sulfur alone on Ni(001) [150], Fe monolayers on Ni(111) [151], Ag monolayers on MgO(001) [152], Au-capped Fe monolayers on MgO(001) [153], NO adsorption on Rh, Pd and Pt [154], and Li on Ru(001) [155]. Typical properties predicted are the equilibrium positions, magnetic moments, charge densities and surface densities of states.

More recently, other groups—primarily in Europe—have begun doing pseudopotential plane wave (often gradient-corrected) DFT supercell slab calculations (figure B3.2.12(D)) for chemisorption on metals. The groups of Nørskov [156], Scheffler [157], Baerends [158, 159] and Hafner and Kresse [160, 161] have been the most active. Adsorbate–metal surface systems examined include: alkalis and N_2 on Ru [156], NO on Pd [156], H_2 on Al [156], Cu [156, 158], Pd [157, 158] and sulfur-covered Pd [157], CO oxidation on Ru [157], CO on Ni, Pd and Pt [158], O on Pt [160], and H_2 on Rh, Pd and Ag [161].

An interesting study by te Velde and Baerends [159] compared slab- and cluster-DFT results for CO absorption on Cu(100). They found large oscillations in the chemisorption binding energy of CO to finite copper clusters as a function of cluster size. This suggests that the finite-cluster model (figure B3.2.12(E)) is likely to be inadequate, at least for modelling metal surfaces. By contrast, the slab calculations converge quickly with the number of Cu layers for the CO heat of adsorption and CO–CO distances.

The supercell plane wave DFT approach is periodic in three dimensions, which has some disadvantages: (i) thick vacuum layers are required so the slab does not interact with its images, (ii) for a tractably sized unit cell, only high adsorbate coverages are modelled readily and (iii) one is limited in accuracy by the form of the exchange–correlation functional chosen. In particular, while DFT, especially using gradient-corrected forms of the exchange–correlation functional (GGA), has proven to be remarkably reliable in many instances, there are a number of examples for chemisorption in which the commonly used GGAs have been shown to fail dramatically (errors in binding energies of $\sim$1 eV or greater) [162, 163]. This naturally motivates the next set of approaches, namely the embedded cluster strategy.

B3.2.4.5 Embedded-cluster schemes: cluster in cluster

Whitten and co-workers developed a metal cluster embedding scheme appropriate for CI calculations during the 1980s [164]. In essence, the method consists of: (i) solving for a HF minimum basis set (one 4s orbital/atom) description of a large cluster (e.g., $\sim$30–90 atoms); (ii) localizing the orbitals *via* exchange energy maximization with atomic basis functions on the periphery; (iii) using these localized orbitals to set up effective Coulomb and exchange operators for the electrons within the cluster to be embedded; (iv) improving the basis set on the atoms comprising the embedded cluster and (v) performing a small CI calculation ($O(10^3)$ configurations) within orbitals localized on the embedded cluster. This strategy provides an approximate way of accounting for nearby electrons outside the embedded cluster itself. Whitten and co-workers have applied it to a variety of adsorbates (H, N, O, C—containing small molecules) on, primarily, Ni surfaces. Duarte and Salahub recently reported a DFT-cluster-in-DFT-cluster variant of Whitten's embedding, with a couple of twists on the original approach (for example, fractional orbital occupancies and charges, and an

extra buffer region) [165]. Earlier, Sellers developed a related scheme for embedding a MP2 cluster within another cluster, where the background was modelled with screened ECPs [166]. Also, Ravenek and Geurts [167] and Fukunishi and Nakatsuji [168] extended the Green's matrix method of Pisani [169] (who developed it mainly for ionic crystals) to again embed a cluster within a cluster by introducing a semiorthogonal basis and renormalizing the charge on the cluster. It was implemented within the X_α method in the former case [167], and by broadening each discrete energy level to mimic the bulk band structure within HF theory for the cluster in the latter case [168].

Pisani [169] has used the density of states from periodic HF (see B3.2.2.4) slab calculations to describe the host in which the cluster is embedded, where the applications have been primarily to ionic crystals such as LiF. The original calculation to derive the external Coulomb and exchange fields is usually done on a finite cluster and at a low level of *ab initio* theory (typically minimum basis set HF, one electron only per atom treated explicitly).

The main drawback of the cluster-in-cluster methods is that the embedding operators are derived from a wavefunction that does not reflect the proper periodicity of the crystal: a two-dimensionally infinite wavefunction/density with a proper band structure would be preferable. Indeed, Rösch and co-workers pointed out recently a series of problems with such cluster-in-cluster embedding approaches. These include the lack of marked improvement of the results over finite clusters of the same size, problems with the orbital space partitioning such that charge conservation is violated, spurious mixing of virtual orbitals into the density matrix [170], the inherent delocalized nature of metallic orbitals [171], etc.

B3.2.4.6 Embedding of clusters in periodic background

One of the first cluster embedding schemes was put forth by Ellis and co-workers [172]. They were interested in studying transition metal impurities in NiAl alloys, so they considered a $TMAl_xNi_y$ cluster embedded in a periodic self-consistent crystal field appropriate for bulk β'-NiAl. The field was calculated via X_α calculations, as was the cluster itself. The idea was to provide a relatively inexpensive alternative to supercell DFT calculations.

Perhaps the most sophisticated embedding scheme for describing metal surfaces to date is the LDA-based self-consistent Green's function method for semi-infinite crystals. Inglesfield, Benesh, and co-workers embed the near-surface layers using an embedding potential constructed from the bulk Green's function within an all-electron approach, using an LAPW basis [173]. Scheffler and co-workers developed a similar approach using a Gaussian basis for the valence electrons and pseudopotentials [174]. The formulation of the latter method is somewhat different from Inglesfield's and Benesh's, in that a reference system is chosen for which the Green's function and density are known (typically the bulk metal), and a Δ(Green's function) is solved for in order to get a Δ(embedding potential) and hence a Δ(density). This allows one to solve for the embedding potential locally in a small region around the adsorbate. These methods allow for an economical yet accurate calculation of the embedding density, which yields a trustworthy description of charge transfer and other equilibrium properties, though subject to the accuracy limitations inherent in DFT-LDA.

In the late 1980s, Feibelman developed his Green's function scattering method using LDA with pseudopotentials to describe adsorption on two-dimensionally infinite metal slabs [175], based on earlier work by Williams *et al* [176]. The physical basis for the technique is that the adsorbate may be considered a defect off which the Bloch waves of the perfect substrate scatter. The interaction region is short-range because of screening by the electron gas of the metal. Feibelman has used this technique to study, for example, the chemisorption of an H_2 molecule on Rh(001) [177], S adatoms on Al(331) [178] and Ag adatoms on Pt(111) [179]. Charge densities, relative energies for various adsites and diffusion barriers (the latter in good agreement with experiment) were the typical quantities predicted.

Krüger and Rösch implemented within DFT the Green's matrix approach of Pisani within an approximate periodic slab environment [180]. They were able to successfully extend Pisani's embedding approach to metal

surfaces by smoothing out the step function that determines the occupation numbers near the Fermi level. Keys to the numerical success of their method included: (i) symmetric orthogonalization of the Bloch basis to produce a localized set of functions that yielded a balanced distribution of charge in the system and (ii) self-consistent evaluation of the Fermi energy by fixing the charge on the cluster to be neutral. The slab was described with a Slater basis at the DFT-LDA level, while the embedded cluster orbitals were expanded in terms of Gaussian functions at the DFT-LDA level. While some properties exhibited non-monotonic behaviour with increasing cluster size, the charge transfer between the metal surface and the adsorbate seemed to be well described. They concluded that properties are not well converged in this method if the cluster does not contain shells of metal atoms that are at least next-nearest-neighbours to the adsite metal atoms.

Head and Silva used occupation numbers obtained from a periodic HF density matrix for the substrate to define localized orbitals in the chemisorption region, which then defines a cluster subspace on which to carry out HF calculations [181]. Contributions from the surroundings also only come from the bare slab, as in the Green's matrix approach. Increases in computational power and improvements in minimization techniques have made it easier to obtain the electronic properties of adsorbates by supercell slab techniques, leading to the Green's function methods becoming less popular [182].

Cortona embedded a DFT calculation in an orbital-free DFT background for ionic crystals [183], which necessitates evaluation of kinetic energy density functionals (KEDFs). Wesolowski and Warshel [184] had similar ideas to Cortona, except they used a frozen density background to examine a solute in solution and examined the effect of varying the KEDF. Stefanovich and Truong also implemented Cortona's method with a frozen density background and applied it to, for example, water adsorption on NaCl(001) [185].

B3.2.4.7 Embedding explicit correlation methods in a DFT background

In principle, DFT calculations with an ideal exchange–correlation functional should provide consistently accurate energetics. The catch is, of course, that the exact exchange–correlation functional is not known. While various GGAs have been remarkably successful, there are notable exceptions [186, 187], including ones specific to surface adsorption mentioned earlier, where the binding-energy errors can be more than an eV [162, 163]. As another example, Louie and Cohen and co-workers found no systematic improvement over the LDA when gradient corrections were included in calculations of Al, Nb and Pd bulk properties, including the cohesive energy [186]. Indeed, the design of exchange–correlation functionals constitutes an active field of research (see, for example, [188]). The lack of completely systematic means to improve these functionals is an unappealing aspect of these calculations.

A first step towards a systematic improvement over DFT in a local region is the method of Aberenkov *et al* [189], who calculated a correlated wavefunction embedded in a DFT host. However, this is achieved using an analytic embedding potential function fitted to DFT results on an indented crystal. One must be cautious using a bare indented crystal to represent the surroundings, since the density at the surface of the indented crystal will have inappropriate Friedel oscillations inside and decay behaviour at the indented surface not present in the real crystal.

We have developed a different first-principles embedding theory that combines DFT with explicit correlation methods. We sought to develop a method for treating bulk or surface phases that is more accurate than current implementations of DFT. The idea is to provide more accurate predictions for local energetics, such as chemisorption binding energies and adsorbate electronic excitation energies. To achieve this, our theory improves upon the DFT description of electron correlation in a local region. This is accomplished by an embedding theory that treats a small region within an accurate quantum chemistry approach [190, 191], which interacts with its surroundings *via* an embedding potential, $v_{\mathrm{embed}}(r)$. This $v_{\mathrm{embed}}(r)$ is derived from a periodic DFT calculation on the total system. It is expressed purely in terms of orbital-free DFT (kinetic and potential energy) interaction terms between the embedded region and its surroundings *à la* Cortona and, in particular, purely in terms of functionals of the total density, ρ_{tot}, and the density of the embedded region,

ρ_I. We thus avoid construction of localized orbitals to describe the electrons in the surrounding environment. This is especially important for metal surfaces, where the extensive k-point sampling required to get a well converged density makes localization impractical (very expensive). This way of expressing the embedding operator also eliminates problems that occur in other forms of embedding, such as those of matching conditions at the embedding boundary, or spurious charge transfer, since the electrostatic potential and the density are continuous by construction. Its only real disadvantage is that there is an arbitrariness associated with the choice of T_s. Development of optimal T_s functionals is an active area of research in our group [97–99].

The self-consistent embedding cycle proceeds as follows. First, a well converged density, ρ_{tot}, is calculated for the extended metal surface in the presence of an adsorbate. This is accomplished within a standard pseudopotential plane wave DFT calculation (see chapter A1.3). Second, we partition the system into the region of interest (typically the adsorbate and neighbouring metal atoms at or near the surface) and its surroundings (all the other atoms in the periodic unit cell). The embedded region is defined by the integral number of electrons and nuclei within that region but not by a particular physical, fixed boundary. This allows for the electron density from the embedded region to expand or contract variationally into the surroundings, thus affording some effective charge polarization to occur as needed.

The electron density, ρ_I, of the embedded cluster/adsorbate atoms is calculated using quantum chemistry methods (HF, PT, multireference SCF, or CI). The initial step in this iterative procedure sets $v_{embed}(r)$ to zero, since ρ_I is needed in order to calculate it. On subsequent iterations, the third step is to use ρ_I and ρ_{tot} to calculate $v_{embed}(r)$, then insert it, as a one-electron operator expressed in matrix form in the atomic orbital basis of the adsorbate/cluster, into the quantum chemistry calculation of step two, and then ρ_I is updated (*via* the wavefunction). We repeatedly update $v_{embed}(r)$ and then ρ_I until full self-consistency is achieved, with fixed ρ_{tot}. In this way, we variationally optimize both the quantum chemistry wavefunction and, implicitly, the density of the surroundings, subject to fixed ρ_{tot}. We tacitly assume that the DFT-slab density for the total system, ρ_{tot}, is in fact a good representation and does not need to be adjusted.

We have shown that our embedding total energies may be written in terms of the total energy obtained in step one (the DFT total energy for the entire system), plus a correction term, that subtracts out the DFT energy in the local region I and adds back in an *ab initio* total energy for that same region,

$$E_{tot}^{embed} = E_{tot}^{DFT} + (E_I^{ab\,initio} - E_I^{DFT}).$$

Thus, another way to think of the embedding is that the *ab initio* treatment of region I is *correcting* the DFT results in the same region, for the same self-consistent density. We expect, then, that such a treatment should reduce, for example, the famous LDA overbinding problem (LDA bond energies are generally significantly overestimated). We have indeed seen a smooth decrease in the LDA overbinding as a function of increasing electron correlation. We benchmarked the method against nearly exact calculations on a small system and then further corroborated it on experimentally well studied chemisorption systems: CO on transition metal surfaces. Our binding energies are in good agreement with nearly full configuration interaction in the former and experimental adsorbate binding energies in the latter. Very recently, we have demonstrated that excitation energies for adsorbed CO are dramatically improved compared to experiment upon inclusion of the embedding potential [192]. In the future, we hope this method will provide a general means for accurate predictions of the local electronic structure of condensed matter.

B3.2.5 Outlook

Computational solid-state physics and chemistry are vibrant areas of research. The all-electron methods for high-accuracy electronic structure calculations mentioned in section B3.2.3.2 are in active development, and with PAW, an efficient new all-electron method has recently been introduced. Ever more powerful computers enable more detailed predictions on systems of increasing size. At the same time, new, more complex materials require methods that are able to describe their large unit cells and diverse atomic make-up. Here, the new

orbital-free DFT method may lead the way. More powerful techniques are also necessary for the accurate treatment of surfaces and their interaction with atoms and, possibly complex, molecules. Combined with recent progress in embedding theory, these developments make possible increasingly sophisticated predictions of the quantum structural properties of solids and solid surfaces.

Acknowledgments

The authors would like to thank Professor P E Blöchl, Dr H Eckstein, Professor W Schattke, Professor K E Smith and T Strasser for making figures available for this publication. FS thanks Dr E E Krasovskii for introducing him to the LAPW method.

References

[1] Whitten J L and Yang H 1996 Theory of chemisorption and reactions on metal surfaces *Surf. Sci. Rep.* **24** 59–124
[2] Mehl M J and Papaconstantopoulos D A 1998 Tight-binding parametrization of first-principles results *Topics in Computational Materials Science* ed C Y Fong (Singapore: World Scientific);
URL http://cst-www.nrl.navy.mil/~mehl/review/rev4.html
[3] Starrost F, Bornholdt S, Solterbeck C and Schattke W 1996 Band-structure parameters by genetic algorithm *Phys. Rev.* B **53** 12 549; *Phys. Rev.* B **54** 17 226E
Strasser T, Starrost F, Solterbeck C and Schattke W 1997 Valence-band photoemission from GaN(001) and GaAs: GaN surfaces *Phys. Rev.* B **56** 13 326
[4] Klimeck G, Brown R C, Boykin T B, Salazar-Lazaro C, Cwik T A and Stoica A 2000 Si tight-binding parameters from genetic algorithm fitting *Superlattices Microstruct.* **27** 10
Klimeck G, Brown R C, Boykin T B, Salazar-Lazaro C, Cwik T A and Stoica A 1999 *Preprint* 1006/spmi.1999.0797
[5] Cohen R E, Mehl M J and Papaconstantopoulos D A 1994 Tight-binding total-energy method for transition and noble metals *Phys. Rev.* B **50** 14 694–7
[6] Haas H, Wang C Z, Fähnle M, Elsässer C and Ho K M 1998 Environment-dependent tight-binding model for molybdenum *Phys. Rev.* B **57** 1461
[7] Harrison W A 1989 *Electronic Structure and the Properties of Solids* (New York: Dover)
[8] Menon M and Subbaswamy K R 1994 Transferable nonorthogonal tight-binding scheme for silicon *Phys. Rev.* B **50** 11 577
[9] Slater P C and Koster G F 1954 Simplified LCAO method for the periodic potential problem *Phys. Rev.* **94** 1498–524
[10] Mehl M J and Papaconstantopoulos D A 1996 Applications of a tight-binding total-energy method for transition and noble metals: Elastic constants, vacancies and surfaces of monatomic metals *Phys. Rev.* B **54** 4519
Mazin I I, Papaconstantopoulos D A and Singh D J 2000 Tight-binding Hamiltonians for Sr-filled ruthenates: Application to the gap anisotropy and Hall coefficient in Sr_2RuO_4 *Phys. Rev.* B **61** 5223
[11] Mercer J L Jr and Chou M Y 1994 Tight-binding model with intra-atomic matrix elements *Phys. Rev.* B **49** 8506
[12] Watson S C, Carter E A, Walters M K and Madden P A (unpublished)
[13] Seifert G, Eschrig H and Bieger W 1986 An approximate variation of the LCAO-Xα method *Z. Phys. Chem.* **267** 529
[14] Horsfield A P 1997 Efficient *ab initio* tight binding *Phys. Rev.* B **56** 6594–602
[15] Elstner M, Porezag D, Jungnickel G, Elsner J, Haugk M, Frauenheim Th, Suhai S and Seifert G 1998 Self-consistent-charge density-functional tight-binding method for simulations of complex materials properties *Phys. Rev.* B **58** 7260
[16] Lee S M, Belkhir M A, Zhu X Y, Lee Y H, Huang Y G and Frauenheim Th 2000 Electronic structure of GaN edge dislocations *Phys. Rev.* B **61** 16 033
[17] Bowler D R, Aoki M, Goringe C M, Horsfield A P and Pettifor D G 1997 A comparison of linear scaling tight-binding methods *Modelling Simulation Mater. Sci. Eng.* **5** 199
[18] Wang C S and Callaway J 1978 BNDPKG. A package of programs for the calculation of electronic energy bands by the LCGO method *Comput. Phys. Commun.* **14** 327
[19] Voß D, Krüger P, Mazur A and Pollmann J 1999 Atomic and electronic structure of WSe_2 from *ab initio* theory: bulk crystal and thin film systems *Phys. Rev.* B **60** 14 311
[20] Artacho E, Sánchez-Portal D, Ordejón P, García A and Soler J M 1999 Linear-scaling *ab initio* calculations for large and complex systems *Phys. Status Solidi* B **215** 809
[21] Hoffmann R 1963 An extended Hückel theory. I. Hydrocarbons *J. Chem. Phys.* **39** 1397
[22] Henk J, Schattke W, Carstensen H, Manzke R and Skibowski M 1993 Surface-barrier and polarization effects in the photoemission from GaAs(110) *Phys. Rev.* B **47** 2251
[23] Strasser T, Solterbeck C, Starrost F and Schattke W 1999 Valence-band photoemission from the GaN(0001) surface *Phys. Rev.* B **60** 11 577
[24] Hohenberg P and Kohn W 1964 Inhomogeneous electron gas *Phys. Rev.* **136** B864
[25] Kohn W and Sham L J 1965 Self-consistent equations including exchange and correlation effects *Phys. Rev.* **140** A1133

[26] Janak J F 1978 Proof that $\partial E/\partial n_i = \varepsilon_i$ in density-functional theory *Phys. Rev.* B **18** 7165–8
[27] Perdew J P, Parr R G, Levy M and Balduz J L Jr 1982 Density-functional theory for fractional particle number: derivative discontinuities of the energy *Phys. Rev. Lett.* **49** 1691–4
Kleinman L 1997 Significance of the highest occupied Kohn–Sham eigenvalue *Phys. Rev.* B **56** 12 042–5
Perdew J P and Levy M 1997 Comment on 'Significance of the highest occupied Kohn–Sham eigenvalue' *Phys. Rev.* B **56** 16 021–8
Kleinman L 1997 Reply to 'Comment on 'Significance of the highest occupied Kohn–Sham eigenvalue'' *Phys. Rev.* B **56** 16 029–30
[28] Bechstedt F 1992 Quasiparticle corrections for energy gaps in semiconductors *Adv. Solid State Phys.* **32** 161
[29] Fiorentini V and Baldereschi A 1995 Dielectric scaling of the self-energy scissor operator in semiconductors and insulators *Phys. Rev.* B **51** 17 196
[30] Pulci O, Onida G, Shkrebtii A I, Del Sole R and Adolph B 1997 Plane-wave pseudopotential calculation of the optical properties of GaAs *Phys. Rev.* B **55** 6685
[31] Hedin L and Lundqvist S 1969 Effects of electron–electron and electron–phonon interactions on the one-electron states of solids *Solid State Phys.* **23** 1
[32] Hybertsen M S and Louie S G 1985 First-principles theory of quasiparticles: Calculation of band gaps in semiconductors and insulators *Phys. Rev. Lett.* **55** 1418
[33] Louie S G 1987 Theory of quasiparticle energies and excitation spectra of semiconductors and insulators *Electronic Band Structure and Its Applications (Lecture Notes in Physics vol 283)* ed M Youssouf (Berlin: Springer)
[34] Rohlfing M, Krüger P and Pollmann J 1997 Quasiparticle calculations of semicore states in Si, Ge, and CdS *Phys. Rev.* B **56** R7065–8
[35] Godby R W, Schlüter M and Sham L J 1988 Self-energy operators and exchange–correlation potentials in semiconductors *Phys. Rev.* B **37** 10159–75
[36] Massidda S, Continenza A, Posternak M and Baldereschi A 1997 Quasiparticle energy bands of transition-metal oxides within a model GW scheme *Phys. Rev.* B **55** 13 494–502
[37] Shirley E L 1998 Many-body effects on bandwidths in ionic, noble gas, and molecular solids *Phys. Rev.* B **58** 9579–83
[38] Rieger M M and Godby R W 1998 Charge density of semiconductors in the GW approximation *Phys. Rev.* B **58** 1343
[39] Campillo I, Silkin V M, Pitarke J M, Chulkov E V, Rubio A and Echenique P M 2000 First-principles calculations of hot-electron lifetimes in metals *Phys. Rev.* B **61** 13 484–92
[40] Perdew J P and Zunger A 1981 Self-interaction correction to density-functional approximations for many-electron systems *Phys. Rev.* B **23** 5048
[41] Svane A and Gunnarsson O 1990 Transition-metal oxides in the self-interaction-corrected density-functional formalism *Phys. Rev. Lett.* **65** 1148
[42] Szotek Z, Temmerman W M and Winter H 1993 Application of the self-interaction correction to transition-metal oxides *Phys. Rev.* B **47** 4029
[43] Svane A, Temmerman W and Szotek Z 1999 Theory of pressure-induced phase transitions in cerium chalcogenides *Phys. Rev.* B **59** 7888
[44] Vogel D, Krüger P and Pollmann J 1997 Structural and electronic properties of group-III nitrides *Phys. Rev.* B **55** 12 836, and references therein
[45] Stampfl C, van de Walle C G, Vogel D, Krüger P and Pollmann J 2000 Native defects and impurities in InN: First-principles studies using the local-density approximation and self-interaction and relaxation-corrected pseudopotentials *Phys. Rev.* B **61** R7846–9
[46] Terakura K, Williams A R, Oguchi T and Kübler J 1984 Transition-metal monoxides: Band or Mott insulators *Phys. Rev. Lett.* **52** 1830
Terakura K, Oguchi T, Williams A R and Kübler J 1984 Band theory of insulating transition-metal monoxides: Band-structure calculations *Phys. Rev.* B **30** 4734
[47] Aryasetiawan F and Gunnarson O 1995 Electronic structure of NiO in the GW approximation *Phys. Rev. Lett.* **74** 3221
[48] Anisimov V I, Kuiper P and Nordgren J 1994 First-principles calculation of NiO valence spectra in the impurity-Anderson-model approximation *Phys. Rev.* B **50** 8257–65
[49] Anisimov V I, Aryasetiawan F and Liechtenstein A I 1997 First-principles calculations of the electronic structure and spectra of strongly correlated systems: The LDA+U method *J. Phys.: Condens. Matter* **9** 767
[50] Anisimov V I, Zaanen J and Andersen O K 1991 Band theory and Mott insulators: Hubbard *U* instead of Stoner *I* *Phys. Rev.* B **44** 943
[51] Gunnarsson O, Andersen O K, Jepsen O and Zaanen J 1989 Density-functional calculation of the parameters in the Anderson model: Application to Mn in CdTe *Phys. Rev.* B **39** 1708–22
Anisimov V I and Gunnarsson O 1991 Density-functional calculation of effective Coulomb interactions in metals *Phys. Rev.* B **43** 7570–4
[52] Kwon S K and Min B I 2000 Unquenched large orbital magnetic moment in NiO *Phys. Rev.* B **62** 73
[53] Slater J C 1937 Wave functions in a periodic potential *Phys. Rev.* **51** 846
[54] Singh D J 1994 *Planewaves, Pseudopotentials and the LAPW Method* (Norwell, MA: Kluwer)
[55] Marcus P M 1967 Variational methods in the computation of energy bands *Int. J. Quantum Chem.* **1 S** 567
[56] Koelling D D 1970 Alternative augmented-plane-wave technique: theory and application to copper *Phys. Rev.* B **2** 290–8

[57] Bross H, Bohn G, Meister G, Schubö W and Stöhr H 1970 New version of the modified augmented-plane wave method *Phys. Rev.* B **2** 3098–103
[58] Andersen O K 1975 Linear methods in band theory *Phys. Rev.* B **12** 3060
[59] Singh D and Krakauer H 1991 H-point phonon in molybdenum: Superlinearized augmented-plane-wave calculations *Phys. Rev.* B **43** 1441–5
[60] Krasovskii E E, Yaresko A N and Antonov V N 1994 Theoretical study of ultraviolet photoemission spectra of noble metals *J. Electron Spectrosc. Relat. Phenom.* **68** 157
[61] Sjöstedt E, Nordström L and Singh D J 2000 An alternative way of linearizing the augmented plane-wave method *Solid State Commun.* **114** 15
[62] Shick A B, Liechtenstein A I and Pickett W E 1999 Implementation of the LDA+U method using the full-potential linearized augmented plane-wave basis *Phys. Rev.* B **60** 10 763
[63] Massidda S, Posternak M and Baldereschi A 1993 Hartree–Fock LAPW approach to the electronic properties of periodic systems *Phys. Rev.* B **48** 5058
[64] Koelling D D and Arbman G O 1975 Use of energy derivative of the radial solution in an augmented plane wave method: application to copper *J. Phys. F: Met. Phys.* **5** 2041
[65] Krasovskii E E 1997 Accuracy and convergence properties of the extended linear augmented-plane-wave method *Phys. Rev.* B **56** 12 866
[66] Krasovskii E E, Nemoshkalenko V V and Antonov V N 1993 On the accuracy of the wavefunctions calculated by LAPW method *Z. Phys.* B **91** 463
[67] Singh D 1991 Ground-state properties of lanthanum: treatment of extended-core states *Phys. Rev.* B **43** 6388
[68] Krasovskii E E and Schattke W 1995 The extended-LAPW-based $k^* p$ method for complex bandstructure calculations *Solid State Commun.* **93** 775
[69] Krasovskii E E, Starrost F and Schattke W 1999 Augmented Fourier components method for constructing the crystal potential in self-consistent band-structure calculations *Phys. Rev.* B **59** 10 504
[70] Wimmer E, Krakauer H, Weinert M and Freeman A J 1981 Full-potential self-consistent linearized-augmented-plane-wave method for calculating the electronic structure of molecules and surfaces: O_2 molecule *Phys. Rev.* B **24** 864
[71] Weinert M 1981 Solution of Poisson's equation: beyond Ewald-type methods *J. Math. Phys.* **22** 2433
[72] Petersen M, Wagner F, Hufnagel L, Scheffler M, Blaha P and Schwarz K 2000 Improving the efficiency of FP-LAPW calculations *Comp. Phys. Commun.* **126** 294–309
[73] Asato M, Settels A, Hoshino T, Asada T, Blügel S, Zeller R and Dederichs P H 1999 Full-potential KKR calculations for metals and semiconductors *Phys. Rev.* B **60** 5202
[74] Korringa J 1947 On the calculation of the energy of a Bloch wave in a metal *Physica (Amsterdam)* **13** 392–400
[75] Kohn W and Rostoker N 1954 Solution of the Schrödinger equation in periodic lattices with an application to metallic lithium *Phys. Rev.* **94** 1111–20
[76] Drittler B, Weinert M, Zeller R and Dederichs P H 1991 Vacancy formation energies of fcc transition metals calculated by a full potential Green's function method *Solid State Commun.* **79** 31
[77] Podloucky R, Zeller R and Dederichs P H 1980 Electronic structure of magnetic impurities calculated from first principles *Phys. Rev.* B **22** 5777
[78] Yussouff M 1987 Fast self-consistent KKR method *Electronic Band Structure and Its Applications (Lecture Notes in Physics vol 283)* ed M Yussouff (Berlin: Springer) pp 58–76
[79] Tank R W and Arcangeli C 2000 An introduction to the third-generation LMTO method *Phys. Status Solidi* B **217** 89
[80] Methfessel M, Rodriguez C O and Andersen O K 1989 Fast full-potential calculations with a converged basis of atom-centered linear muffin-tin orbitals: structural and dynamic properties of silicon *Phys. Rev.* B **40** 2009–12
[81] Blöchl P E 1994 Projector augmented-wave method *Phys. Rev.* B **50** 17 953
[82] Holzwarth N A W, Matthews G E, Dunning R B, Tackett A R and Zeng Y 1997 Comparison of the projector augmented-wave, pseudopotential and linearized augmented-plane-wave formalisms for density-functional calculations of solids *Phys. Rev.* B **55** 2005
[83] Alfè D, Kresse G and Gillan M J 2000 Structure and dynamics of liquid iron under Earth's core conditions *Phys. Rev.* B **61** 132
[84] Ohtsuki T, Ohno K, Shiga K, Kawazoe Y, Maruyama Y and Masumoto K 1998 Insertion of Xe and Kr atoms into C60 and C70 fullerenes and the formation of dimers *Phys. Rev. Lett.* **81** 967–70
[85] Krasovska O V, Krasovskii E E and Antonov V N 1995 *Ab initio* calculation of the optical and photoelectron properties of RuO_2 *Phys. Rev.* B **52** 11 825
[86] Leventi-Peetz A, Krasovskii E E and Schattke W 1995 Dielectric function and local field effects of $TiSe_2$ *Phys. Rev.* B **51** 17 965
[87] Traving M, Boehme M, Kipp L, Skibowski M, Starrost F, Krasovskii E E, Perlov A and Schattke W 1997 Electronic structure of WSe_2: a combined photoemission and inverse photoemission study *Phys. Rev.* B **55** 10 392–9
[88] Starrost F, Krasovskii E E, Schattke W, Jockel J, Simon U, Adelung R and Kipp L 2000 Cetineites: electronic, optical, and conduction properties of nanoporous chalcogenoantimonates *Phys. Rev.* B **61** 15 697
[89] Krasovskii E E and Schattke W 1997 Surface electronic structure with the linear methods of band theory *Phys. Rev.* B **56** 12 874
[90] Fisher A J and Blöchl P E 1993 Adsorption and scanning-tunneling-microscope imaging of benzene on graphite and MoS_2 *Phys. Rev. Lett.* **70** 3263–6

[91] Goedecker S 1999 Linear scaling electronic structure methods *Rev. Mod. Phys.* **71** 1085
[92] Galli G 2000 Large-scale electronic structure calculations using linear scaling methods *Phys. Status Solidi* B **217** 231
[93] Fattebert J-L and Bernholc J 2000 Towards grid-based O(N) density-functional theory methods: optimized nonorthogonal orbitals and multigrid acceleration *Phys. Rev.* B **62** 1713–22
[94] Wang L-W and Teter M P 1992 Kinetic-energy functional of the electron density *Phys. Rev.* B **45** 13 196–220
[95] Perrot F 1994 Hydrogen–hydrogen interaction in an electron gas *J. Phys.: Condens. Matter* **6** 431–46
[96] Smargiassi E and Madden P A 1994 Orbital-free kinetic-energy functionals for first-principles molecular dynamics *Phys. Rev.* B **49** 5220–6
[97] Wang Y A and Carter E A 2000 Orbital-free kinetic-energy density functional theory *Theoretical Methods in Condensed Phase Chemistry (Progress in Theoretical Chemistry and Physics Series)* ed S D Schwartz (Boston: Kluwer) pp 117–84
[98] Wang Y A, Govind N and Carter E A 1998 Orbital-free kinetic energy functionals for the nearly-free electron gas *Phys. Rev.* B **58** 13 465
Wang Y A, Govind N and Carter E A 1999 *Phys. Rev.* B **60** 17 162E
[99] Wang Y A, Govind N and Carter E A 1999 Orbital-free kinetic-energy density functionals with a density-dependent kernel *Phys. Rev.* B **60** 16 350
[100] Watson S, Jesson B J, Carter E A and Madden P A 1998 *Ab initio* pseudopotentials for orbital-free density functional *Europhys. Lett.* **41** 37–42
[101] Anta J A, Jesson B J and Madden P A 1998 Ion–electron correlations in liquid metals from orbital-free *ab initio* molecular dynamics *Phys. Rev.* B **58** 6124–32
[102] Jesson B J, Foley M and Madden P A 1997 Thermal properties of the self-interstitial in aluminum: an *ab initio* molecular-dynamics study *Phys. Rev.* B **55** 4941–6
[103] Aoki M I and Tsumuraya K 1997 *Ab initio* molecular-dynamics study of pressure-induced glass-to-crystal transitions in the sodium system *Phys. Rev.* B **56** 2962–8
[104] Watson S C and Carter E A 2000 Linear-scaling parallel algorithms for the first principles treatment of metals *Comp. Phys. Commun.* **128** 67–92
[105] Hedin L 1965 New method for calculating the one-particle Green's function with application to the electron–gas problem *Phys. Rev.* **139** A796
[106] Pisani C, Dovesi R and Roetti C 1988 *Hartree–Fock Ab Initio Treatment of Crystalline Systems (Lecture Notes in Chemistry, vol 48)* (Berlin: Springer)
[107] CRYSTAL98 is the current version of the commercial HF program developed at the University of Torino and at Daresbury Laboratory (http://www.dl.ac.uk/TCS/Software/CRYSTAL/)
[108] Su Y-S, Kaplan T A, Mahanti S D and Harrison J F 1999 Crystal Hartree–Fock calculations for La_2NiO_4 and La_2CuO_4 *Phys. Rev.* B **59** 10 521–9
[109] Fu L, Yaschenko E, Resca L and Resta R 1999 Hartree–Fock studies of surface properties of $BaTiO_3$ *Phys. Rev.* B **60** 2697–703
[110] Causà M, Dovesi R and Roetti C 1991 Pseudopotential Hartree–Fock study of seventeen III-V and IV-IV semiconductors *Phys. Rev.* B **43** 11 937–43
[111] Chartier A, D'Arco P, Dovesi R and Saunders V R 1999 *Ab initio* Hartree–Fock investigation of the structural, electronic, and magnetic properties of Mn_3O_4 *Phys. Rev.* B **60** 14 042–8, and references therein
[112] McMillan W L 1965 Ground state of liquid ^{4}He *Phys. Rev.* **138** A442
[113] Ceperly D M and Kalos M H 1986 Quantum many-body problems, *Monte Carlo Methods in Statistical Physics (Topics in Current Physics, vol 7)* 2nd edn, ed K Binder (Berlin: Springer) pp 145–94
[114] Rajagopal G, Needs R J, James A, Kenney S D and Foulkes W M C 1995 Variational and diffusion quantum Monte Carlo calculations at nonzero wave vectors: theory and application to diamond-structure germanium *Phys. Rev.* B **51** 10 591–600
[115] Umrigar C J, Wilson K G and Wilkins J W 1988 Optimized trial wavefunctions for quantum Monte Carlo calculations *Phys. Rev. Lett.* **60** 1719–22
[116] Metropolis N, Rosenbluth A W, Rosenbluth M N, Teller A H and Teller E 1953 Equation of state calculations by fast computing machines *J. Chem. Phys.* **21** 1087
[117] Kent P R C, Hood R Q, Williamson A J, Needs R J, Foulkes W M C and Rajagopal G 1999 Finite-size errors in quantum many-body simulations of extended systems *Phys. Rev.* B **59** 1917–29
[118] Eckstein H, Schattke W, Reigrotzki M and Redmer R 1996 Variational quantum Monte Carlo ground state of GaAs *Phys. Rev.* B **54** 5512–15
[119] Hammond B L, Lester W A and Reynolds P J 1994 *Monte Carlo Methods in Ab Initio Quantum Chemistry* (Singapore: World Scientific)
[120] Ceperly D M and Alder B J 1980 Ground state of the electron gas by a stochastic method *Phys. Rev. Lett.* **45** 566–9
[121] Towler M D, Hood R Q and Needs R J 2000 Minimum principles and level splitting in quantum Monte Carlo excitation energies: application to diamond *Phys. Rev.* B **62** 2330–7
[122] Filippi C and Umrigar C J 2000 Correlated sampling in quantum Monte Carlo: a route to forces *Phys. Rev.* B **61** R16 291
[123] Alfè D, Gillan M J and Price G D 2000 Constraints on the composition of the Earth's core from *ab initio* calculations *Nature* **405** 172–5

[124] Upton T H and Goddard W A III 1981 Chemisorption of H, Cl, Na, O, and S atoms on Ni(100) surfaces: a theoretical study using Ni_{20} clusters *Crit. Rev. Solid State Mater. Sci.* **10** 261–96

[125] Bagus P S, Bauschlicher C W Jr, Nelin C J, Laskowski B C and Seel M 1984 A proposal for the proper use of pseudopotentials in molecular orbital cluster model studies of chemisorption *J. Chem. Phys.* **81** 3594–602

[126] Panas I, Schüle J, Siegbahn P and Wahlgren U 1988 On the cluster convergence of chemisorption energies *Chem. Phys. Lett.* **149** 265–72

Siegbahn P E M, Nygren M A and Wahlgren U 1992 *Cluster Models for Surface and Bulk Phenomena* ed G Pacchioni, P S Bagus and F Parmigiani *(NATO ASI Series B: Physics vol 283)* (New York: Plenum) p 267

[127] Panas I, Siegbahn P and Wahlgren U 1989 The mechanism for the O_2 dissociation on Ni(100) *J. Chem. Phys.* **90** 6791–801

[128] Fournier R and Salahub D R 1990 Chemisorption and magnetization: A bond order-rigid band model *Surf. Sci.* **238** 330–40

Ushio J, Papai I, St-Amant A and Salahub D R 1992 Vibrational analysis of formate adsorbed on Ni(110): LCGTO-MCP-LSD study *Surf. Sci.* **262** L134–8

[129] Mlynarski P and Salahub D R 1991 Local and nonlocal density functional study of Ni_4 and Ni_5 clusters. Models for the chemisorption of hydrogen on (111) and (100) nickel surfaces *J. Chem. Phys.* **95** 6050–6

[130] Papai I, Salahub D R and Mijoule D 1990 An LCGTO=MCP-LSD study of the (2 × 1) H-covered Pd(110) surface *Surf. Sci.* **236** 241–9

[131] Rochefort A, Andzelm J, Russo N and Salahub D R 1990 Chemisorption and diffusion of atomic hydrogen in and on cluster models of Pd, Rh, and bimetallic PdSn, RhSn, and RhZn catalysts *J. Am. Chem. Soc.* **112** 8239–47

[132] Bagus P S and Pacchioni G 1995 Ionic and covalent electronic states for K adsorbed on Cu_5 and Cu_{25} cluster models of the Cu(100) surface *J. Chem. Phys.* **102** 879

[133] Clotet A and Pacchioni G 1996 Acetylene on Cu and Pd(111) surfaces: A comparative theoretical study of bonding mechanism, adsorption sites, and vibrational spectra *Surf. Sci.* **346** 91

[134] Bauschlicher C W Jr 1994 A theoretical study of CO/Cu(100) *J. Chem. Phys.* **101** 3250

[135] Triguero L, Wahlgren U, Boussard P and Siegbahn P 1995 Calculations of hydrogen chemisorption energies on optimized Cu clusters *Chem. Phys. Lett.* **237** 550

[136] Illas F, Zurita S, Marquez A M and Rubio J 1997 On the bonding mechanism of CO to Pt(111) and its effect on the vibrational frequency of chemisorbed CO *Surf. Sci.* **376** 279

[137] Illas F, Rubio J, Ricart J M and Pacchioni G 1996 The importance of correlation effects on the bonding of atomic oxygen on Pt(111) *J. Chem. Phys.* **105** 7192

[138] Rochefort A, McBreen P and Salahub D R 1996 Bond selectivity in the dissociative adsorption of c-CH_2N_2 on single crystals: a comparative DFT-LSD investigation for Pd(110) and Cu (110) *Surf. Sci.* **347** 11

[139] Filali Baba M, Mijoule C, Godbout N and Salahub D R 1994 Coadsorption of K and CO on Pd clusters: a density functional study *Surf. Sci.* **316** 349

[140] Kantorovich L N 1988 An embedded-molecular-cluster method for calculating the electronic structure of point defects in non-metallic crystals. I. General theory *J. Phys. C: Solid State Phys.* **21** 5041

Meng J, Pandey R, Vail J M and Kunz A B 1989 Impurity potentials derived from embedded quantum clusters: Ag^+ and Cu^+ transport in alkali halides *J. Phys.: Condens. Matter* **1** 6049–58

Grimes R W, Catlow C R A and Stoneham A M 1989 A comparison of defect energies in MgO using Mott–Littleton and quantum mechanical procedures *J. Phys.: Condens. Matter* **1** 7367–84

Zuo J, Pandey R and Kunz A B 1991 Embedded-cluster study of the lithium trapped-hole center in magnesium oxide *Phys. Rev.* B **44** 7187–91

Zuo J, Pandey R and Kunz A B 1992 Embedded-cluster study of Cu^+-induced lattice relaxation in alkali halides *Phys. Rev.* B **45** 2709–11

Visser O, Visscher L, Aerts P J C and Nieuwpoort W C 1992 Molecular open shell configuration interaction calculations using the Dirac–Coulomb Hamiltonian: the f^6-manifold of an embedded EuO_6^{9-} cluster *J. Chem. Phys.* **96** 2910–19

Pisani C, Orlando R and Cora F 1992 On the problem of a suitable definition of the cluster in embedded-cluster treatments of defects in crystals *J. Chem. Phys.* **97** 4195–204

Martin R L, Pacchioni G and Bagus P S 1992 *Cluster Models for Surface and Bulk Phenomena* ed G Pacchioni *et al (NATO ASI Series B: Physics vol 283)* (New York: Plenum) p 485

Martin R L, Pacchioni G and Bagus P S 1992 *Cluster Models for Surface and Bulk Phenomena* ed G Pacchioni *et al (NATO ASI Series B: Physics vol 283)* (New York: Plenum) p 305

Pisani C 1993 Embedded-cluster techniques for the quantum-mechanical study of surface reactivity *J. Mol. Catal.* **82** 229

Hermann K 1992 *Cluster Models for Surface and Bulk Phenomena* ed G Pacchioni *et al (NATO ASI Series B: Physics vol 283)* (New York: Plenum) p 209

[141] Nakatsuji H 1987 Dipped adcluster model for chemisorptions and catalytic reactions on metal surface *J. Chem. Phys.* **87** 4995–5001

Nakatsuji H and Nakai H 1990 Theoretical study on molecular and dissociative chemisorptions of an O_2 molecule on an Ag surface: dipped adcluster model combined with symmetry-adapted cluster-configuration interaction method *Chem. Phys. Lett.* **174** 283–6

Nakatsuji H, Nakai H and Fukunishi Y 1991 Dipped adcluster model for chemisorptions and catalytic reactions on a metal surface: Image force correction and applications to Pd-O_2 adclusters *J. Chem. Phys.* **95** 640–7

Nakatsuji H and Nakai H 1992 Dipped adcluster model study for the end-on chemisorption of O_2 on an Ag surface *Can. J. Chem.* **70** 404–8

Nakatsuji H, Kuwano R, Morita H and Nakai H 1993 Dipped adcluster model and SAC-CI method applied to harpooning, chemical luminescence and electron emission in halogen chemisorption on alkali metal surface *J. Mol. Catal.* **82** 211–28

Zhen-Ming Hu and Nakatsuji H 1999 Adsorption and disproportionation reaction of OH on Ag surfaces: dipped adcluster model study *Surf. Sci.* **425** 296–312

[142] Nakatsuji H 1997 Dipped adcluster model for chemisorption and catalytic reactions *Prog. Surf. Sci.* **54** 1

[143] Chang T-M, Martinez T J and Carter E A 1994 unpublished results

[144] Rösch N, Sandl P, Gorling A and Knappe P 1988 Toward a chemisorption cluster model using the LCGTO-Xα method: application to Ni(100)/Na *Int. J. Quantum Chem. Symp.* **22** 275

[145] Weinelt M, Huber W, Zebisch P, Steinrück H-P, Ulbricht P, Birkenheuer U, Boettger J C and Rösch N 1995 The adsorption of acetylene on Ni(110): an experimental and theoretical study *J. Chem. Phys.* **102** 9709

[146] Pacchioni G, Chung S-C, Krüger S and Rösch N 1997 Is CO chemisorbed on Pt anomalous compared with Ni and Pd? An example of surface chemistry dominated by relativistic effects *Surf. Sci.* **392** 173

[147] Staufer M *et al* 1999 Interpretation of x-ray emission spectra: NO adsorbed on Ru(001) *J. Chem. Phys.* **111** 4704–13

[148] Weinert M, Wimmer E and Freeman A J 1982 Total-energy all-electron density functional method for bulk solids and surfaces *Phys. Rev.* B **26** 4571–8

Jansen H J F and Freeman A J 1984 Total-energy full-potential linearized augmented plane-wave method for bulk solids: electronic and structural properties of tungsten *Phys. Rev.* B **30** 561–9

[149] Wimmer E, Fu C L and Freeman A J 1985 Catalytic promotion and poisoning: all-electron local-density-functional theory of CO on Ni(001) surfaces coadsorbed with K or S *Phys. Rev. Lett.* **55** 2618–21

[150] Fu C L and Freeman A J 1989 Covalent bonding of sulfur on Ni(001): S as a prototypical adsorbate catalytic poisoner *Phys. Rev.* B **40** 5359

[151] Wu R and Freeman A J 1992 Structural and magnetic properties of Fe/Ni(111) *Phys. Rev.* B **45** 7205

[152] Li C, Wu R, Freeman A J and Fu C L 1993 Energetics, bonding mechanism, and electronic structure of metal–ceramic interfaces: Ag/MgO(001) *Phys. Rev.* B **48** 8317–22

[153] Wu R and Freeman A J 1994 Magnetism at metal–ceramic interfaces: effects of a Au overlayer on the magnetic properties of Fe/MgO(001) *J. Magn. Magn. Mater.* **137** 127–33

[154] Mannstadt W and Freeman A J 1997 Dynamical and geometrical aspects of NO chemisorption on transition metals: Rh, Pd, and Pt *Phys. Rev.* B **55** 13 298

[155] Mannstadt W and Freeman A J 1998 LDA theory of the coverage dependence of the local density of states: Li adsorbed on Ru(001) *Phys. Rev.* B **57** 13 289

[156] Mortensen J J, Hammer B and Norskov J K 1998 Alkali promotion of N_2 dissociation over Ru(0001) *Phys. Rev. Lett.* **80** 4333

Hammer B and Norskov J K 1997 Adsorbate reorganization at steps: NO on Pd(211) *Phys. Rev. Lett.* **79** 4441

Hammer B, Scheffler M, Jacobsen K W and Norskov J K 1994 Multidimensional potential energy surface for H_2 dissociation over Cu(111) *Phys. Rev. Lett.* **73** 1400

Gundersen K, Jacobsen K W, Norskov J K and Hammer B 1994 The energetics and dynamics of H_2 dissociation on Al(110) *Surf. Sci.* **304** 131

[157] Wei C M, Gross A and Scheffler M 1998 *Ab initio* calculation of the potential energy surface for the dissociation of H_2 on the sulfur-covered Pd(100) surface *Phys. Rev.* B **57** 15 572

Tomanek D, Wilke S and Scheffler M 1997 Hydrogen-induced polymorphism of the Pd(110) surface *Phys. Rev. Lett.* **79** 1329

Stampfl C and Scheffler M 1997 Mechanism of efficient carbon monoxide oxidation at Ru(0001) *J. Vac. Sci. Technol.* A **15** 1635

Stampfl C and Scheffler M 1997 Anomalous behavior of Ru for catalytic oxidation: a theoretical study of the catalytic reaction CO+1/2 O_2 to CO_2 *Phys. Rev. Lett.* **78** 1500

Stampfl C and Scheffler M 1996 Theoretical study of O adlayers on Ru(0001) *Phys. Rev.* B **54** 2868

[158] Philipsen P H T, van Lenthe E, Snijders J G and Baerends E J 1997 Relativistic calculations on the adsorption of CO on the (111) surfaces of Ni, Pd and Pt within the zeroth-order regular approximation *Phys. Rev.* B **56** 13 556

Olsen R A, Philipsen P H T, Baerends E J, Kroes G J and Louvik O M 1997 Direct subsurface adsorption of hydrogen on Pd(111): quantum mechanical calculations on a new two-dimensional potential energy surface *J. Chem. Phys.* **106** 9286

Wiesenekker G, Kroes G J and Baerends E J 1996 An analytical six-dimensional potential energy surface for dissociation of molecular hydrogen on Cu(100) *J. Chem. Phys.* **104** 7344

Philipsen P H T, te Velde G and Baerends E J 1994 The effect of density-gradient corrections for a molecule-surface potential energy surface. Slab calculations on Cu(100)c(2x2)-CO *Chem. Phys. Lett.* **226** 583

[159] te Velde G and Baerends E J 1993 Slab versus cluster approach for chemisorption studies, CO on Cu(100) *Chem. Phys.* **177** 399

[160] Feibelman P J, Hafner J and Kresse G 1998 Vibrations of O on stepped Pt(111) *Phys. Rev.* B **58** 2179–84

[161] Eichler A, Kresse G and Hafner J 1998 Ab-initio calculations of the 6D potential energy surfaces for the dissociative adsorption of H_2 on the (100) surfaces of Rh, Pd and Ag *Surf. Sci.* **397** 116–36

[162] Rösch N 1998 *Lecture Given at the 7th International Symposium on Theoretical Aspects of Heterogeneous Catalysis, Cambridge, 25-28 August*

[163] Hammer B, Hansen L B and Nørskov J K 1999 Improved adsorption energetics within density functional theory using revised Perdew–Burke–Enerhof functionals *Phys. Rev.* B **59** 7413–21

[164] Whitten J L and Pakkanen T A 1980 Chemisorption theory for metallic surfaces: Electron localization and the description of surface interactions *Phys. Rev.* B **21** 4357–67

Madhavan P and Whitten J L 1982 Theoretical studies of the chemisorption of hydrogen on copper *J. Chem. Phys.* **77** 2673–83

Cremaschi P and Whitten J L 1987 The effect of hydrogen chemisorption on titanium surface bonding *Theor. Chim. Acta.* **72** 485–96

Whitten J L 1992 *Cluster Models for Surface and Bulk Phenomena* ed G Pacchioni *et al (NATO ASI Series B: Physics vol 283)* (New York: Plenum) p 375

Whitten J L 1993 Theoretical studies of surface reactions: embedded cluster theory *Chem. Phys.* **177** 387–97

[165] Duarte H A and Salahub D R 1998 Embedded cluster model for chemisorption using density functional calculations: oxygen adsorption on the Al(100) surface *J. Chem. Phys.* **108** 743

[166] Sellers H 1991 On modeling chemisorption processes with metal cluster systems. II. Model atomic potentials and site specificity of N atom chemisorption on Pd(111) *Chem. Phys. Lett.* **178** 351–7

[167] Ravenek W and Geurts F M M 1986 Hartree–Fock–Slater–LCAO implementation of the moderately large-embedded-cluster approach to chemisorption. Calculations for hydrogen on lithium (100) *J. Chem. Phys.* **84** 1613–23

[168] Fukunishi Y and Nakatsuji H 1992 Modifications for *ab initio* calculations of the moderately large-embedded-cluster model. Hydrogen adsorption on a lithium surface *J. Chem. Phys.* **97** 6535–43

[169] Pisani C 1978 Approach to the embedding problem in chemisorption in a self-consistent-field-molecular-orbital formalism *Phys. Rev.* B **17** 3143

Pisani C, Dovesi R and Nada R 1990 *Ab initio* Hartree–Fock perturbed-cluster treatment of local defects in crystals *J. Chem. Phys.* **92** 7448

Pisani C 1993 Embedded-cluster techniques for the quantum-mechanical strudy of surface reactivity *J. Mol. Catal.* **82** 229

Casassa S and Pisani C 1995 Atomic-hydrogen interaction with metallic lithium: an *ab initio* embedded-cluster study *Phys. Rev.* B **51** 7805

[170] Gutdeutsch U, Birkenheuer U, Krüger S and Rösch N 1997 On cluster embedding schemes based on orbital space partitioning *J. Chem. Phys.* **106** 6020

[171] Gutdeutsch U, Birkenheuer U and Rösch N 1998 A strictly variational procedure for cluster embedding based on the extended subspace approach *J. Chem. Phys.* **109** 2056

[172] Ellis D E, Benesh G A and Byrom E 1978 Self-consistent embedded-cluster model for magnetic impurities: β'-NiAl *J. Appl. Phys.* **49** 1543

Ellis D E, Benesh G A and Byrom E 1979 Self-consistent embedded-cluster model for magnetic impurities: Fe, Co, and Ni in β'-NiAl *Phys. Rev.* B **20** 1198

[173] Benesh G A and Inglesfield J E 1984 An embedding approach for surface calculations *J. Phys. C: Solid State Phys.* **17** 1595

Inglesfield J E and Benesh G A 1988 Surface electronic structure: embedded self-consistent calculations *Phys. Rev.* B **37** 6682

Aers G C and Inglesfield J E 1989 Electric field and Ag(001) surface electronic structure *Surf. Sci.* **217** 367

Colbourn E A and Inglesfield J E 1991 Effective charges and surface stability of O on Cu(001) *Phys. Rev. Lett.* **66** 2006

Crampin S, van Hoof J B A N, Nekovee M and Inglesfield J E 1992 Full-potential embedding for surfaces and interfaces *J. Phys.: Condens. Matter* **4** 1475

Benesh G A and Liyanage L S G 1994 Surface-embedded Green-function method for general surfaces: application to Al(111) *Phys. Rev.* B **49** 17 264

Trioni M I, Brivio G P, Crampin S and Inglesfield J E 1996 Embedding approach to the isolated adsorbate *Phys. Rev.* B **53** 8052–64

[174] Scheffler M, Droste Ch, Fleszar A, Maca F, Wachutka G and Barzel G 1991 A self-consistent surface-Green-function (SSGF) method *Physica* B **172** 143

Wachutka G, Fleszar A, Maca F and Scheffler M 1992 Self-consistent Green-function method for the calculation of electronic properties of localized defects at surfaces and in the bulk *J. Phys.: Condens. Matter* **4** 2831

Bormet J, Neugebauer J and Scheffler M 1994 Chemical trends and bonding mechanisms for isolated adsorbates on Al(111) *Phys. Rev.* B **49** 17 242

Wenzien B, Bormet J and Scheffler M 1995 Green function for crystal surfaces I *Comp. Phys. Commun.* **88** 230

[175] Feibelman P J 1987 Force and total-energy calculations for a spatially compact adsorbate on an extended, metallic crystal surface *Phys. Rev.* B **35** 2626

[176] Williams A R, Feibelman P J and Lang N D 1982 Green's-function methods for electronic-structure calculations *Phys. Rev.* B **26** 5433

[177] Feibelman P J 1991 Orientation dependence of the hydrogen molecule's interaction with Rh(001) *Phys. Rev. Lett.* **67** 461

[178] Feibelman P J 1994 Sulfur adsorption near a step on Al *Phys. Rev.* B **49** 14 632

[179] Feibelman P J 1994 Diffusion barrier for a Ag adatom on Pt(111) *Surf. Sci.* **313** L801

[180] Krüger S and Rösch N 1994 The moderately-large-embedded-cluster method for metal surfaces; a density-functional study of atomic adsorption *J. Phys.: Condens. Matter* **6** 8149

Krüger S, Birkenheuer U and Rösch N 1994 Density functional approach to moderately large cluster embedding for infinite metal substrates *J. Electron Spectrosc. Relat. Phenom.* **69** 31

[181] Head J D and Silva S J 1996 A localized orbitals based embedded cluster procedure for modeling chemisorption on large finite clusters and infinitely extended surfaces *J. Chem. Phys.* **104** 3244
[182] Brivio G P and Trioni M I 1999 The adiabatic molecule–metal surface interaction: theoretical approaches *Rev. Mod. Phys.* **71** 231–65
[183] Cortona P 1991 Self-consistently determined properties of solids without band structure calculations *Phys. Rev.* B **44** 8454
Cortona P 1992 Direct determination of self-consistent total energies and charge densities of solids: A study of the cohesive properties of the alkali halides *Phys. Rev.* B **46** 2008
[184] Wesolowski T A and Warshel A 1993 Frozen density functional approach to *ab initio* calculations of solvated molecules *J. Phys. Chem.* **97** 8050
Wesolowski T A and Warshel A 1994 *Ab initio* free energy perturbation calculations of solvation free energy using the frozen density functional approach *J. Phys. Chem.* **98** 5183
[185] Stefanovich E V and Truong T N 1996 Embedded density functional approach for calculations of adsorption on ionic crystals *J. Chem. Phys.* **104** 2946
[186] Garcia A, Elsässer C, Zhu J, Louie S G and Cohen M L 1992 Use of gradient-corrected functionals in total-energy calculations for solids *Phys. Rev.* B **46** 9829
[187] Nachtigall P, Jordan K D, Smith A and Jónsson H 1996 Investigation of the reliability of density functional methods: reaction and activation energies for Si-Si bond cleavage and H_2 elimination from silanes *J. Chem. Phys.* **104** 148
[188] Perdew J P, Burke K and Ernzerhof M 1996 Generalized gradient approximation made simple *Phys. Rev. Lett.* **77** 3865
Proynov E I, Sirois S and Salahub D R 1997 Extension of the LAP functional to include parallel spin correlation *Int. J. Quantum Chem.* **64** 427
Tozer D J, Handy N C and Green W H 1997 Exchange-correlation functionals from *ab initio* electron densities *Chem. Phys. Lett.* **273** 183
Filatov M and Thiel W 1997 A new gradient-corrected exchange-correlation density functional *Mol. Phys.* **91** 847
van Voorhis T and Scuseria G E 1998 A novel form for the exchange-correlation energy functional *J. Chem. Phys.* **109** 400
Zhang Y and Yang W 1998 *Phys. Rev. Lett.* **80** 890
Tozer D J and Handy N C 1998 The development of new exchange-correlation functionals *J. Chem. Phys.* **108** 2545
[189] Abarenkov I V, Bulatov V L, Godby R, Heine V, Payne M C, Souchko P V, Titov A V and Tupitsyn I I 1997 Electronic-structure multiconfiguration calculation of a small cluster embedded in a local-density approximation host *Phys. Rev.* B **56** 1743
[190] Govind N, Wang Y A, da Silva A J R and Carter E A 1998 Accurate *ab initio* energetics of extended systems via explicit correlation embedded in a density functional environment *Chem. Phys. Lett.* **295** 129
[191] Govind N, Wang Y A and Carter E A 1999 Electronic structure calculations by first principles density-based embedding of explicitly correlated systems *J. Chem. Phys.* **110** 7677
[192] Kluener T, Wang Y A, Govind N and Carter E A 2000 in preparation
[193] Rubio A, Corkill J L, Cohen M L, Shirley E L and Louie S G 1993 Quasiparticle band structure of AlN and GaN *Phys. Rev.* B **48** 11 810–16
[194] Dhesi S S, Stagarescu C B, Smith K E, Doppalapudi D, Singh R and Moustakas T D 1997 Surface and bulk electronic structure of thin-film wurtzite GaN *Phys. Rev.* B **56** 10 271–5
[195] Starrost F 1999 *PhD Thesis* Christian-Albrechts-Universität Kiel
Starrost F, Krasovskii E E and Schattke W 1999 unpublished
[196] Günther O, Janowitz C, Jungk G, Jenichen B, Hey R, Däweritz L and Ploog K 1995 Comparison between the electronic dielectric functions of a GaAs/AlAs superlattice and its bulk components by spectroscopic ellipsometry using core levels *Phys. Rev.* B **52** 2599–609
[197] Starrost F, Krasovskii E E and Schattke W 1998 An alternative full-potential ELAPW method *Verhandl. DPG (VI)* **33** 741
[198] Aspnes D E and Studna A A 1983 Dielectric functions and optical parameters of Si, Ge, GaP, GaAs, GaSb, InP, InAs, and InSb from 1.5 to 6.0 eV *Phys. Rev.* B **27** 985–1009
[199] Logothetidis S, Alouani M, Garriga M and Cardona M 1990 E_2 interband transitions in $Al_xGa_{1-x}As$ alloys *Phys. Rev.* B **41** 2959–65
[200] Hughes J L P and Sipe J E 1996 Calculation of second-order optical response in semiconductors *Phys. Rev.* B **53** 10 751–63
[201] Wang C S and Klein B M 1981 First-principles electronic structure of Si, Ge, GaP, GaAs, ZnS and ZnSe. II. Optical properties *Phys. Rev.* B **24** 3417–29
[202] Huang Ming-Zhu and Ching W Y 1993 Calculation of optical excitations in cubic semiconductors. I. Electronic structure and linear response *Phys. Rev.* B **47** 9449–63

Further Reading

Pisani C (ed) 1996 *Quantum-Mechanical Ab-initio Calculation of the Properties of Crystalline Materials (Lecture Notes in Chemistry vol 67)* (Berlin: Springer)

A general introduction.

Dreizler R M and Gross E K U 1990 *Density Functional Theory: an Approach to the Quantum Many-body Problem* (Berlin: Springer)

A monograph on the foundations of density functional theory.

Pisani C, Doves R and Roetti C 1988 *Hartree–Fock Ab Initio Treatment of Crystalline Systems (Lecture Notes in Chemistry vol 48)* (Berlin: Springer)

An introduction to periodic Hartree–Fock.

Nemoshkalenko V V and Antonov V N 1998 *Computational Methods in Solid State Physics* (Amsterdam: Gordon and Breach)

An explicit introduction to the all-electron methods.

Singh D J 1994 *Planewaves, Pseudopotentials and the LAPW Method* (Norwell, MA: Kluwer)

A textbook on plane-wave and LAPW methods.

Whitten J L and Yang H 1996 Theory of chemisorption and reactions on metal surfaces *Surf. Sci. Rep.* **24** 59–124